2008

Synchrotron radiation from laser-electron interactions : measurement and modeling

V. A. (Vladimir Aleksandrovich) Semenov
San Jose State University

SYNCHROTRON RADIATION FROM LASER-ELECTRON INTERACTIONS: MEASUREMENT AND MODELING

A Thesis

Presented to

The Faculty of the Department of Physics

San Jose State University

In Partial Fulfillment

of the Requirements for the Degree

Master of Science

by

Vladimir Alexandrovich Semenov

December 2008

APPROVED FOR THE DEPARTMENT OF PHYSICS

Dr. Kenneth Wharton, Asst. Professor

Dr. Carel Boekema, Professor

Dr. Alejandro Garcia, Professor

APPROVED FOR THE UNIVERSITY

ABSTRACT

SYNCHROTRON RADIATION FROM LASER-ELECTRON INTERACTIONS:

MEASUREMENT AND MODELING

by Vladimir A. Semenov

Synchrotron radiation emitted by electrons due to laser-plasma interactions is an important tool in researching those interactions. The features of this radiation can provide insights into electrons' collective and individual behavior. The basic theory of single electron motion due to a laser pulse is reviewed. Further, the radiation emitted by a collection of the electrons is modeled. The experimental set-up for the detection of this radiation is presented, and the results are compared to a theoretical model.

ACKNOWLEDGMENTS

I spent 12 months working on this project. Sometimes it was hard. Sometimes it was easy. But it was always a great deal of fun. I would like to thank all the people who were around me during that time. Without them I would not have been able to get the results I got.

First and foremost I would like to thank Dwight Price for his time and expertise. One look at the problem is usually all it takes for him to solve it. Thank you very much for all of your help.

I want to thank my thesis advisor, Dr. Ken Wharton, for making the whole project possible, for guiding and teaching me during the project as well as for helping me with the modeling of the results and the writing of the thesis. Thank you very much for your optimism and good cheer.

I thank John Boyett for all of his time and help with the laser.

I also would like to thank Tommy Chang, Andrew MacKinnon, Andrew Ng, and Klaus Widman, for their interest in, support of, and discussion of my project.

Josie Morgado, thank you very much for the help with all the paperwork.

TABLE OF CONTENTS

LIST OF TABLES

LIST OF FIGURES

1.0. INTRODUCTION

Beginning in the mid-1960s, several advances in laser design gradually increased the peak power output of lasers. Q-switching, mode-locking and finally Chirped-Pulse Amplification made possible the creation of table-top high-energy ultra-short pulse lasers. By the beginning of the 1990s, irradiances of ExaWatts (10^{18} per cm^2) became possible. Those irradiances allowed for study of a new regime of laser-matter interactions, because the electrons in the laser focus became relativistic.

In this work we present a study of interaction between high power laser light and electrons in plasma. The motivation and outline of the project are considered in the introduction. Theoretical descriptions of single electron motion, radiation from a single electron and interference of radiation from many electrons follow. Chapter 3 of this thesis focuses on features of the experimental setup. Finally, results are presented and discussed.

In 2002, Kaplan and Shkolnikov introduced an idea of "Lasetron" – an attosecond x-ray source. The reasoning behind the suggestion is that a single electron moving in such a fashion would radiate mostly in the direction of its velocity. In fact, for relativistic electrons, radiation is confined to the cone around the velocity vector. The angle between the velocity vector and the edge of that cone is $1/\gamma$ where $\gamma = \sqrt{1 - u^2/c^2}$ is the relativistic parameter for an electron with velocity u. Thus, a stationary observer would receive radiation from the electron only once per revolution. This observer would observe a

series of ultra-short bursts of radiation from the electron. The duration of each burst is given by:

$$\tau = \frac{2}{\gamma \cdot \omega} \tag{1.1}$$

Where ω is the angular frequency of incident light.

Such a source would in principle allow for time resolution of nuclear processes. There are several questions that need to be answered before such a source could be, in principle, feasible. Radiation emitted by a single electron would be very difficult to detect. Fortunately, there is more than one electron in the plasma. If N electrons were to move in a way described above then one would expect the intensity of radiation to be higher. Let us assume that all electrons move in phase. Then each of them would produce a certain electric field at the point of observation at certain times. Electric fields from different electrons would add up arithmetically. The intensity of radiation is proportional to the square of the electric field, so the intensity of the radiation detected would scale as N^2. Thus, radiation from coherently moving electrons could reach detectable levels for a relatively small number of electrons.

Therefore, it is clear that all electrons need to be moving coherently for radiation to be detectable. This assumption has been challenged. Among the authors challenging it are Stupakov and Zolotarev (2002), Kaplan and Shkolnikov (2002), Garnett (2002). Furthermore, in the noisy environment of plasma-laser interactions there are many effects that might destroy the needed coherence in an electron's motion. Thus, testing whatever electrons are indeed, moving coherently is crucial in the development of short x-ray

sources both for Lasetron and other proposals. The proposals are made by Earsley, Ride, and Sprangle (1993), K. Lee et al. (2003) and Lee, Kim, and Kim. (2005).

The experiment we present studies the interaction between a laser pulse and high density plasma. The laser beam (USP laser system) is circularly polarized and focused down to a 5 micron spot. The wavelength of the laser is $800nm$. Energies of up to 1J are observed, while the pulse duration is around $140fs$. Those parameters create energy densities of up to $1.07 \cdot 10^{19} W/cm^2$. The laser beam is focused on a metal target. However, the profile of the pulse is more complex than a simple Gaussian with an appropriate time constant. Before the main pulse of that shape arrives there is a less energetic pre-pulse. This pre-pulse vaporizes the metal target and strips electrons from a significant number of atoms. Those electrons then are driven by the main pulse's electromagnetic field. Let us consider the physics of this process in more detail.

We will start by considering an electron's movement due to its interaction with circularly polarized light. Circularly polarized light has electric and magnetic fields that rotate in a plane perpendicular to the direction of propagation. Let us look at a single electron under such conditions. Assuming that the electron's initial velocity is zero, one can prove that it will move in a circle in the plane perpendicular to the k-vector of the incident laser pulse. The force from the E-field provides centripetal acceleration for the electron's circular motion. The Lorentz force is zero because the electron's velocity is parallel to the magnetic field. The phase and frequency of the electron's movement are determined by the electric field of the incident light.

Let us return to the duration of each as calculated in (1.1). This formula is applicable only if all electrons were to be moving in phase. The phase of the electron as it rotates in a circle is determined by the phase of the electric field. As we travel along the direction of the propagation this phase continuously changes. Every laser pulse is longer than the wavelength of the light in it. Thus the phase of the electric field would go through a change of at least $2 \cdot \pi$. That means that at any given time there will be a plane in which the electric field is perpendicular to the direction of observation. Or, since the electric field provides the centripetal force for our motion, there will be an electron with its velocity pointing in the direction of observation. That means that at any given time there will be electrons that radiate in the direction of observation. The time in interval (1.1) is the duration of the burst due to a single electron. Instead, this analysis predicts a constant radiation with a duration determined by the length of the pulse.

In a circularly polarized laser field, the radiating electrons form a spiral that rotates with the frequency of the incident light. Electrons rotate only around the center of the beam. If an electron were to start its rotation slightly off-center of the laser beam, it would fairly quickly spiral out of the area of interest. The reason for this is that a turning electric field would be smaller in one part of the trajectory, thus failing to return the electron to its initial position after one cycle. The radius of the spiral is determined by the intensity of the electric field. The "pitch" (distance between loops) of the spiral is equal to the wavelength of the incoming light. The length of the spiral is determined by the length of the pulse -- in our case it is at least 50 wavelengths.

The fact that we have a radiating spiral means that there will be interference between the radiations from different parts of the spiral. For each given wavelength there will be constructive or destructive interference for different directions. This interference should result in an angular narrowing of the radiation perpendicular to k-direction. A crude analogy might be drawn comparing our spiral to 50 point sources situated a wavelength apart from each other.

The experiment was conducted at the Ultra Short Pulse (USP) laser facility at Lawrence Livermore National Laboratory. We set out to look for radiation emitted by laser-driven electrons. For the radiation to be detectable, a significant number of electrons need to be moving coherently.

This radiation has been successfully detected. Furthermore, features of the radiation detected give us insight into the collective behavior of electrons. For example, angular spread of the radiation gives a spatial coherence length for the radiating electrons.

In Chapter 2, the theory behind coherent synchrotron radiation from laser-plasma interactions is presented. Relativistic equations of motion for a single electron are derived and solved. Radiation from a single electron is described. A model describing radiation due to the coherent movement of a number of electrons is presented.

Chapter 3 presents the experimental layout and techniques. Laser beam alignment, focusing, polarization measurements and stability analysis are among topics discussed. Laser beam targeting hardware and procedures are outlined. Finally, radiation detection (with special attention to filtering) is described.

Experimental data follows in Chapter 4; row data is presented along with data analysis methods and experimental results. A discussion of the results is followed by outlook and conclusion. Appended are all the row data used in the analysis.

2.0. THEORY

A theoretical explanation of the phenomena observed is given in this chapter. A single electron's motion due to a driving electromagnetic field near the laser's focus is described. Broadband radiation due to this motion is calculated. Finally, interference of broadband radiation due to the coherent multi-electron movement is taken into account. Even though the main thrust of the discussion focuses on circularly polarized laser light as the driving agent, extensions into linearly polarized light are considered.

2.1. Motion of a single electron

It is necessary to find appropriate forms for vector ($\vec{A}$) and scalar (Φ) potentials to describe driving fields. Driving fields are due to light so the Coulomb gauge is very appropriate. In the Coulomb gauge, scalar (electrostatic) potential depends only on charge density distribution. Our plasma is charge-neutral, so charge density is zero everywhere. Thus, Φ vanishes in the Coulomb gauge. Also $\vec{A}$ satisfies the wave equation. All those factors combine to give us fields $\vec{E}$ and $\vec{B}$:

$$\vec{E} = -\frac{d}{dt}\vec{A}$$
$$\vec{B} = \nabla \times \vec{A} \qquad (2.1)$$

From those formulas we derive expressions for $\vec{A}$, $\vec{E}$ and $\vec{B}$ which are self-consistent for the circularly polarized plane wave:

$$\begin{array}{lll} A_x = A_0 \cdot e^{i\cdot(k\cdot z-\omega\cdot t-\pi/2)} & E_x = E_0 \cdot e^{i\cdot(k\cdot z-\omega\cdot t-\pi/2)} & B_x = -B_0 \cdot e^{i\cdot(k\cdot z-\omega\cdot t)} \\ A_y = A_0 \cdot e^{i\cdot(k\cdot z-\omega\cdot t)} & E_y = E_0 \cdot e^{i\cdot(k\cdot z-\omega\cdot t)} & B_y = B_0 \cdot e^{i\cdot(k\cdot z-\omega\cdot t-\pi/2)} \\ A_z = 0 & E_z = 0 & B_z = 0 \end{array} \tag{2.2}$$

Here we directed the z axis along the k-vector of the incoming wave. Formulas describing the linearly polarized wave behave almost exactly like the circularly polarized wave. If we pick the x axis along the direction of polarization then we obtain by setting to zero the y component of $\vec{A}$ and $\vec{E}$; and the x component of $\vec{B}$:

$$\begin{array}{lll} A_x = A_0 \cdot e^{i\cdot(k\cdot z-\omega\cdot t-\pi/2)} & E_x = E_0 \cdot e^{i\cdot(k\cdot z-\omega\cdot t-\pi/2)} & B_x = 0 \\ A_y = 0 & E_y = 0 & B_y = B_0 \cdot e^{i\cdot(k\cdot z-\omega\cdot t-\pi/2)} \\ A_z = 0 & E_z = 0 & B_z = 0 \end{array} \tag{2.2a}$$

It could be shown from (2.1) and (2.2)-(2.2a) that:

$$E_0 = -i \cdot \omega \cdot A_0$$

$$B_0 = i \cdot k \cdot A_0$$

$$B_0 = -\frac{k}{\omega} \cdot E_0 = -\frac{E_0}{c} \tag{2.3}$$

Now we are ready for the relativistic Lagrangian. The single-particle form of the Lagrangian is:

$$L = -m \cdot c^2 \cdot \sqrt{1-\frac{u^2}{c^2}} + \frac{e}{c} \cdot \vec{u} \cdot \vec{A} + e \cdot \Phi \tag{2.4}$$

Where m, e, u are particles' mass, charge and velocity (3D), $\vec{A}$, Φ are vector and scalar potentials of electromagnetic field. As always c is the speed of light. The canonical momentum P_i associated with the coordinate i is:

$$P_i = \frac{d}{du_i} L = \gamma \cdot m \cdot u_i + \frac{e}{c} \cdot A_i \tag{2.5}$$

Fortunately, we don't need to use the general form. $\vec{A}$ doesn't depend on x and y while Φ is zero (we are still working in the Coulomb gauge). Thus x and y coordinates are cyclical. For them, corresponding generalized momenta are conserved. Therefore:

$$\begin{aligned} \gamma(t) \cdot m \cdot u_x(t) &= \gamma(0) \cdot m \cdot u_x(0) + \frac{e}{c} \cdot \left(A_x(0) - A_x(t)\right) \\ \gamma(t) \cdot m \cdot u_y(t) &= \gamma(0) \cdot m \cdot u_y(0) + \frac{e}{c} \cdot \left(A_y(0) - A_y(t)\right) \end{aligned} \tag{2.6}$$

Now, let us consider motion along the z-axis. Partial derivatives of the Lagrangian with respect to u_z and z are:

$$\begin{aligned} \frac{d}{du_z} L &= -m \cdot \frac{u}{\sqrt{1 - \frac{u^2}{c^2}}} + \frac{e}{c} \cdot u_z \cdot A_z \\ \frac{d}{dz} L &= \frac{e}{c} \cdot \vec{u} \cdot \frac{d}{dz} \cdot \vec{A} \end{aligned} \tag{2.7}$$

But A_z is zero and derivatives with respect to z of A_x and A_y are B_y and $-B_x$ respectively (see equation (2.1)). Thus the equation of motion is:

$$\frac{d}{dt} p_z = \frac{e}{c} \cdot (u_x \cdot B_y - u_y \cdot B_x) \tag{2.8}$$

Plugging in for u_x and u_y from 2.6 one derives:

$$\frac{d}{dt}p_z = \frac{B_x(t)\cdot\left(\gamma(0)\cdot u_x(0)+\frac{e}{c}\cdot A_x(0)\right)+B_y(t)\cdot\left(\gamma(0)\cdot u_y(0)+\frac{e}{c}\cdot A_y(0)\right)}{\gamma(t)\cdot m}+ \tag{2.9}$$
$$+\frac{e^2}{\gamma(t)\cdot m\cdot c^2}\cdot\left(A_x(t)\cdot B_y(t)-A_y(t)\cdot B_x(t)\right)$$

Rewriting (2.6) and (2.9) in terms of the momentum's components we obtain the final equations of the motion for the electron in a plane wave:

$$\begin{aligned}
&\frac{d}{dt}p_z(t) = \frac{B_x(t)\cdot p_x(0)+B_y(t)\cdot p_y(0)}{\gamma(t)\cdot m}+\frac{e^2}{\gamma(t)\cdot m\cdot c^2}\cdot\left(A_x(t)\cdot B_y(t)-A_y(t)\cdot B_x(t)\right)\\
&p_x(t) = p_x(0)+\frac{e}{c}\cdot\left(A_x(0)-A_x(t)\right)\\
&p_y(t) = p_y(0)+\frac{e}{c}\cdot\left(A_y(0)-A_y(t)\right)\\
&\gamma(t) = \sqrt{1+\frac{\left|\vec{p}(t)\right|^2}{m^2\cdot c^2}}
\end{aligned} \tag{2.10}$$

The last equation follows from basic relativistic considerations. Numerical solutions to the equations (2.10) are presented below.

First, let's analyze the equations of motion for circular polarization of the laser light (combining 2.2 and 2.10). In the x-y plane in momentum space an electron's trajectory is a combination of steady drift (determined by initial conditions) and circular motion about the drifting center. Noteworthy is the fact that the z-component of momentum has a non-zero time derivative. Thus, an electron would experience acceleration along the z axis as well as along the x and y axes. More careful examination of this acceleration reveals that it is harmonic in nature (since all

corresponding components of $\vec{A}$ and $\vec{B}$ are harmonic according to 2.2). That means that there is no net acceleration along the z axis. To summarize we observe oscillatory motion along the z axis in combination with a steady velocity drift in z and a circular motion in the x-y plane.

In the special case where an electron is at rest initially, we observe no movement along the z axis. Indeed, the first term in the corresponding equation from (2.10) is zero due to the initial conditions – no movement along the x or y axes at time equals zero. The second term in the p_z from equation (2.10) is zero also (plugging in for the corresponding components of $\vec{B}$ and $\vec{A}$ from (2.2) results in factoring out the phase term $1+e^{i\pi}$, which is zero). Thus the original assumptions presented above are true: **If an electron is originally at rest and γ does not change much we will observe circular motion in the x-y plane with a stationary center.**

Let's find parameters for the circular motion. First, we need to find the radius of the circle and electron's velocity as functions of the magnitude of the electric field. The light is circularly polarized so the x-component of the electric field is given by

$$E_x = E_0 \cdot \cos(\omega \cdot t) \tag{2.11}$$

The relativistic equation of motion along the x axis is

$$\frac{d}{dt} p_x = e \cdot E_x \tag{2.12}$$

Plugging in for momentum and electric field

$$\frac{d}{dt}(\gamma \cdot m \cdot V_x) = e \cdot E_0 \cdot \cos(\omega \cdot t) \tag{2.13}$$

We are looking for circular motion with constant speed. Thus γ is constant. Let's try the solution

$$\begin{aligned} V_x &= V_0 \cdot \sin(\omega \cdot t) \\ \gamma \cdot m \cdot \omega \cdot V_0 \cdot \cos(\omega \cdot t) &= e \cdot E_0 \cdot \cos(\omega \cdot t) \end{aligned} \tag{2.14}$$

Repeating the process for the y coordinate and doing a little algebra we derive:

$$\begin{aligned} \gamma &= \sqrt{1+\varepsilon^2} \\ \beta &= \frac{\varepsilon}{\sqrt{1+\varepsilon^2}} \\ \varepsilon &= \frac{e \cdot E_0}{m \cdot \omega \cdot c} \end{aligned} \tag{2.15}$$

For actual laser beams, the amplitude of the electric field doesn't stay constant with radial position. For such beams (also called Gaussian beams) solving Maxwell's equations gives the electric field as:

$$\begin{aligned} E_0 &= E_{\max} \cdot e^{-\left(\frac{z}{a}\right)^2} \cdot \frac{1}{\sqrt{1+\left(\frac{z}{z_0}\right)^2}} \\ z_0 &= \pi \cdot \frac{w_0^2}{\lambda} \end{aligned} \tag{2.16}$$

Where r is distance to the beam's center, z is distance from the narrowest point of the beam (called the "waist"), and w_0 and z_0 are beam parameters (actually those two distances are related by the last equation, so there is only one free parameter).

Let's combine (2.15) and (2.16). First, we need to plug in for the beam parameters -- we measure w_0 and compute z_0 using formula above. Then, we approximate E_0 from the pulse profile and energy. The laser light's frequency is

computed from its wavelength. Figures 1 and 2 show β and γ as functions of z - distance from the focus of the beam along the laser axis. (Calculations were performed with following set of parameters: wavelength of the light of $800nm$, duration of the shot of $140fs$, energy per shot of $1J$, laser focus of $5\mu m$ (FWHM).)

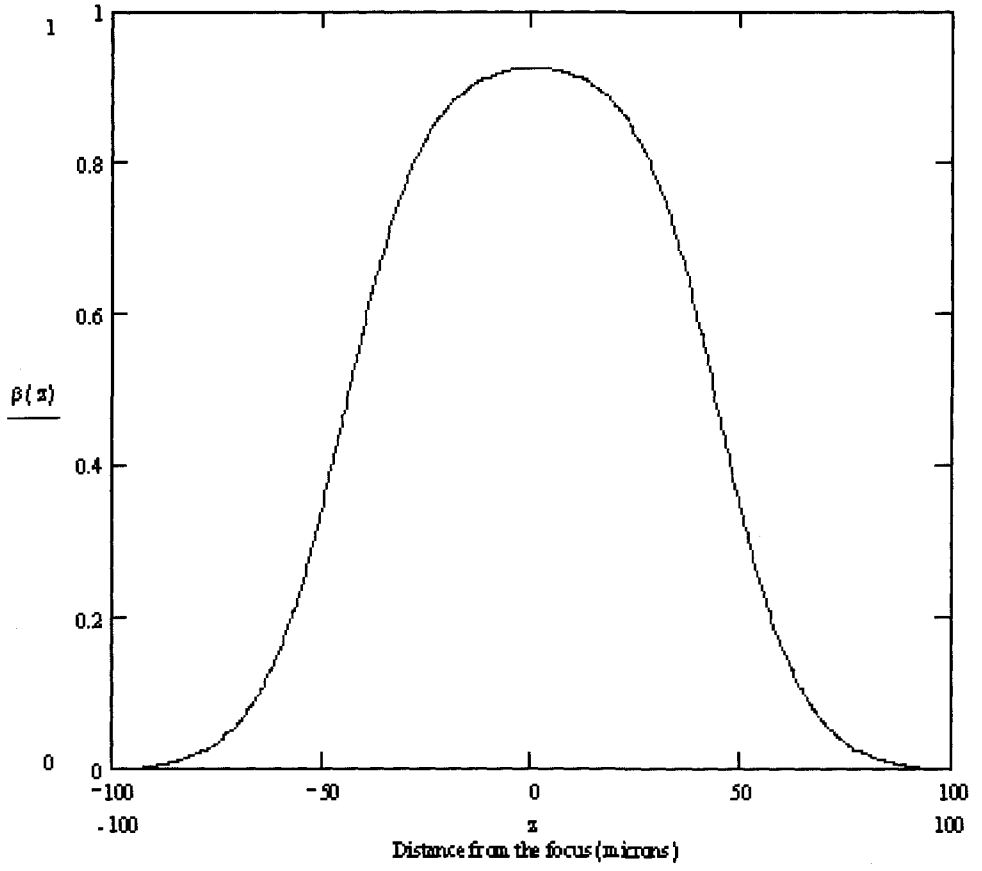

Figure 1. Electron's relativistic velocity ($\beta = v/c$) vs. distance (in μm) from the focus.

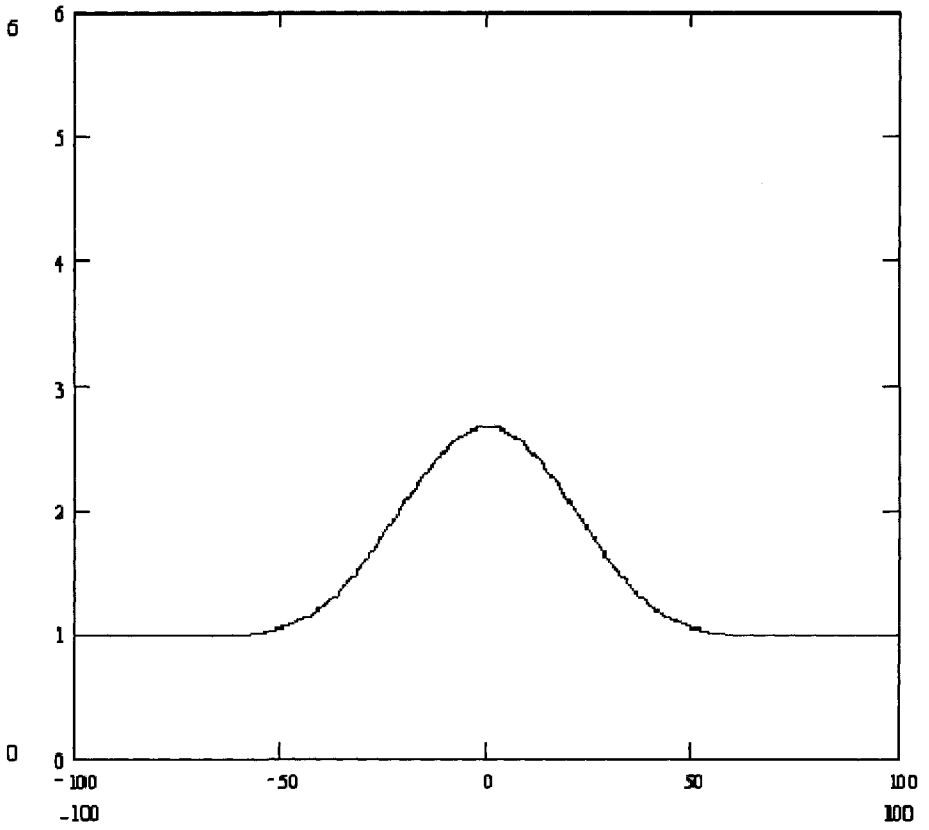

Figure 2. Relativistic parameter $\gamma = 1/\sqrt{1 - v^2/c^2}$ vs. distance (in μm) from the focus.

Now, let us consider the case of linear polarization. Combining equations (2.2a) with the equations of motion (2.10) we obtain the following: p_y stays constant while p_x follows the driving field. Momentum's component p_y is not constant in time, so the electron experiences acceleration along the x and z axes again. The acceleration along the z axis is also non-zero due to the fact that product of velocity and γ is constant (oscillation along the z axis with no net z displacement follows from 2.2a). The coefficient γ changes dramatically now since p_y is sinusoidal in time. That means that u_z has to compensate for that change to keep the momentum along the y axis constant.

Thus, the motion looks like the combination of a drift and periodic motion in the *x-y* plane. Basic Lorenz force consideration leads us to conclude that periodic motion has a form of ∞. Once again, the electron experiences accelerations along all three axes.

There is an alternative (simplified) way to look at the electron's motion due to the linearly polarized driving field. The electric field (by far the biggest force at play) drives electrons to oscillate along its direction. As electrons pick up speed, the $\vec{v} \times \vec{B}$ term begins to contribute, resulting in a small displacement along the magnetic field. Accurate computation of the effect yields a figure ∞ motion along the direction of the electric field. Noteworthy is the fact that a figure ∞ is not significantly different (geometrically) from two circles side by side.

2.2. Radiation of a single moving charge

When dealing with the fields created by a moving charge one has to begin with potentials created by the charge:

$$\Phi(\vec{x},t) = \left[\frac{e}{(1-\vec{\beta}\cdot\vec{n})\cdot R}\right]_{ret}$$
$$\vec{A}(\vec{x},t) = \left[\frac{e\cdot\vec{\beta}}{(1-\vec{\beta}\cdot\vec{n})\cdot R}\right]_{ret} \qquad (2.17)$$

Here R is distance between the charge and the point of observation, $\vec{n}$ is a unit vector pointing from the charge to the point and $\vec{\beta}$ is the charge's velocity. The subscript "ret" means that the quantity in the square brackets should be evaluated at the retarded time t_0. If a charge's trajectory is given by the function $\vec{R}(t)$ then:

$$t_0 = t - \frac{\left|\vec{x} - \vec{R}(t)\right|}{c} \tag{2.18}$$

Using (2.10) and (2.11) one can easily take all the necessary derivatives to compute fields created by a moving charge:

$$\vec{E}(\vec{x},t) = \left[\frac{\vec{n} - \vec{\beta}}{\gamma^2 \cdot (1 - \vec{\beta}\cdot\vec{n})^3 \cdot R^2}\right]_{ret} + \frac{e}{c}\cdot\left[\frac{\vec{n}\times\left[(\vec{n} - \vec{\beta})\times\frac{d}{dt}\vec{\beta}\right]}{(1 - \vec{\beta}\cdot\vec{n})^3 \cdot R}\right]_{ret} \tag{2.19}$$

$$\vec{B}(\vec{x},t) = \left[\vec{n}\times\vec{E}(\vec{x},t)\right]_{ret} \tag{2.20}$$

The two terms in (2.19) vary differently with R. R is the distance between the charge radiating and the point where we observe the radiation. The first term falls off as R squared while the second term – the radiation term – goes down as R. Therefore, the only significant term in the sum above is the second term. Let's consider the energy output of the accelerated charge.

Calculating Poynting's vector from (2.18) is easy: we take cross product of $\vec{B}$ and $\vec{E}$. The radial component of this vector is:

$$\left[\vec{S}\cdot\vec{n}\right]_{ret} = \frac{e^2}{4\cdot\pi\cdot c}\cdot\left[\frac{1}{R^2}\cdot\left(\frac{\vec{\beta}\times\left[(\vec{n} - \vec{\beta})\times\frac{d}{dt}\vec{\beta}\right]}{(1 - \vec{\beta}\cdot\vec{n})^3}\right)\right]_{ret} \tag{2.21}$$

Equations (2.18) and (2.19) give us all the information describing the radiation.

Integrating (2.19) over all possible angles would give us the total power output of the radiating charge. Let's consider radiation from a single charge, moving in a circle with constant speed. To remain consistent with previous remarks we orient the z axis

perpendicular to the plane of the motion. Clearly, the experiment is symmetrical with respect to rotation around the z axis. Thus we can pick the direction of observation along the x axis. Then the three vectors used in (2.18), (2.19) and (2.20) become:

$$\begin{aligned} &\vec{n} = (1,0,0) \\ &\vec{\beta} = \beta_0 \cdot (\cos(\omega \cdot t), \sin(\omega \cdot t), 0) \\ &\frac{d}{dt}\vec{\beta} = \beta_0 \cdot \omega \cdot (-\sin(\omega \cdot t), \cos(\omega \cdot t), 0) \end{aligned} \tag{2.22}$$

Plugging in those vectors gives:

$$\vec{E} = (0,1,0) \cdot \left[\frac{\beta_0 \cdot \omega \cdot (\beta_0 - \cos(\omega \cdot t))}{R \cdot (1 - \beta_0 \cdot \cos(\omega \cdot t))^3} \right]_{ret} \tag{2.23}$$

Finally, we need to find the spectral distribution of intensity for our moving charge. The incoming laser light is $800nm$, in wavelength, while the wavelength at which we detect the radiation is $300nm$ (the actual center wavelength was around $298nm$ but from now on we will round it up to $300nm$ for brevity). This detection wavelength is picked so the frequency of the radiation detected is not a multiple of the frequency of incoming laser light. The plasma could conceivably double or triple the frequency of incoming laser light while redirecting it towards our detector. Tuning off these frequencies we are free to focus on radiation from electrons themselves without detecting substantial noise from the laser-plasma interaction. We need to show that at the frequency corresponding to $300nm$ the spectrum of radiation will have noticeable power.

The power radiated out is given by the radial component of Poynting's vector. Integrating it over time would give us the power output of the radiation from the moving charge. To find the spectral distribution we need to Fourier decompose the radial

component of Poynting's vector and then integrate it over time. Let us consider the particulars.

Here is what this vector looks like (plugging 2.22 into 2.21):

$$\left[\vec{S}\cdot\vec{n}\right]_{ret} = \frac{e^2}{4\cdot\pi\cdot c}\cdot\left[\left(\frac{\beta_0\cdot\omega\cdot(\beta_0-\cos(\omega\cdot t))}{R\cdot(1-\beta_0\cdot\cos(\omega\cdot t))^3}\right)^2\right]_{ret} \tag{2.24}$$

It is easy to see that this function is periodic in time. The Fourier transform of an arbitrary periodical function yields a discreet spectrum. If T is the period of the initial function only frequencies: $\omega_i = i*\frac{2*\pi}{T}$ will have non-zero contributions in the spectrum.

This problem persists even after taking care of retardation. Retarded time t_0 (which we need to substitute for t) is a solution of the equation:

$$t_0 = t - \frac{\left|\vec{x}-\vec{R}(t)\right|}{c} \tag{2.25}$$

However, $\vec{R}(t)$ has the same angular frequency ω. Thus the final function describing the radial component of Poynting's vector will still be periodic in time.

There are two effects which will allow the synchrotron radiation to have off-harmonic ($300nm$) wavelengths. One is that some of the electrons will be moving in the z-direction and will experience a different apparent laser frequency. Also, we need to remember that β_0 - the amplitude of electron's velocity - changes with time. This makes the function described in (2.24) non-periodic. Thus the Fourier component at the

frequency corresponding to $300nm$ is not zero. Let's formalize the ideas discussed above.

Total energy radiated out during the process is given by:

$$Q = \int_{-\infty}^{\infty} \left[\vec{S} \cdot \vec{n}\right]_{ret} \cdot dt = \int_{-\infty}^{\infty} \frac{e^2}{4 \cdot \pi \cdot c} \cdot \left[\left(\frac{\beta_0 \cdot \omega \cdot (\beta_0 - \cos(\omega \cdot t))}{R \cdot (1 - \beta_0 \cdot \cos(\omega \cdot t))^3} \right)^2 \right]_{ret} \cdot dt \tag{2.26}$$

The inverse square R term in the square brackets doesn't change much (the radius of an electron's orbit is around one micron while effective electron-detector distance is at least 10 cm). Thus the $\frac{1}{R^2}$ term could be safely taken out of consideration:

$$Q = \frac{e^2}{4 \cdot \pi \cdot c} \cdot \frac{1}{R^2} \int_{-\infty}^{\infty} \left[\left(\frac{\beta_0 \cdot \omega \cdot (\beta_0 - \cos(\omega \cdot t))}{(1 - \beta_0 \cdot \cos(\omega \cdot t))^3} \right)^2 \right]_{ret} \cdot dt \tag{2.27}$$

We define function F as:

$$F = \left[\left(\frac{\beta_0 \cdot \omega \cdot (\beta_0 - \cos(\omega \cdot t))}{(1 - \beta_0 \cdot \cos(\omega \cdot t))^3} \right) \right]_{ret} \tag{2.28}$$

It is convenient to return back to geometrically more general notation:

$$F = \left[\frac{\vec{n} \times \left((\vec{n} - \vec{\beta}) \times \frac{d}{dt} \cdot \vec{\beta} \right)}{(1 - \vec{\beta} \cdot \vec{n})^3} \right]_{ret} \tag{2.29}$$

Then our energy is:

$$Q = \int_{-\infty}^{\infty} |F|^2 \, dt \tag{2.30}$$

Let's Fourier decompose F and find the coefficient $F(\omega_0)$. Noteworthy is the fact that there are two different angular frequencies here: ω_0 is the frequency of detected radiation while ω is the frequency of the electron's motion. The energy spectrum, i.e. energy radiated at a given frequency, is proportional to that coefficient squared:

$$F(\omega)=\frac{1}{\sqrt{2\cdot\pi}}\cdot\int_{-\infty}^{\infty}F(t)\cdot e^{i\cdot\omega_0\cdot t}\cdot dt=\frac{1}{\sqrt{2\cdot\pi}}\cdot\int_{-\infty}^{\infty}\left[\frac{\vec{n}\times\left((\vec{n}-\vec{\beta})\times\frac{d}{dt}\cdot\vec{\beta}\right)}{(1-\vec{\beta}\cdot\vec{n})^3}\right]_{ret}\cdot e^{i\cdot\omega_0\cdot t}\cdot dt \qquad (2.31)$$

Switching over to the integration over the retarded time t_0 (solution of (2.18)) gives:

$$F(\omega)\frac{1}{\sqrt{2\cdot\pi}}\cdot\int_{-\infty}^{\infty}\left[\frac{\vec{n}\times\left((\vec{n}-\vec{\beta})\times\frac{d}{dt_0}\cdot\vec{\beta}\right)}{(1-\vec{\beta}\cdot\vec{n})^3}\right]\cdot e^{i\cdot\omega_0\cdot\left(t_0+\frac{R(t_0)}{c}\right)}\cdot dt_0 \qquad (2.32)$$

Considerations discussed above let us assume $R(t_0)$ to be constant, thus term $e^{i\cdot\omega_0\cdot\left(t_0+\frac{R(t_0)}{c}\right)}$ would cancel out with its own complex conjugate. Furthermore, direct differentiation will show that:

$$\frac{\vec{n}\times\left((\vec{n}-\vec{\beta})\times\frac{d}{dt_0}\cdot\vec{\beta}\right)}{(1-\vec{\beta}\cdot\vec{n})^2}=\frac{d}{t_0}\left[\frac{\vec{n}\times(\vec{n}\times\vec{\beta})}{(1-\vec{\beta}\cdot\vec{n})}\right] \qquad (2.33)$$

Thus integrating the integral above by parts yields:

$$F(\omega)\frac{1}{\sqrt{2\cdot\pi}}\cdot\int_{-\infty}^{\infty}\vec{n}\times(\vec{n}\times\vec{\beta})\cdot e^{i\cdot\omega_0\cdot t_0}\cdot dt_0 \qquad (2.34)$$

Plugging in for $\vec{\beta}$ and $\vec{n}$ in our coordinate system (2.22) we obtain:

$$F(\omega)\frac{1}{\sqrt{2\cdot\pi}}\cdot\int_{-\infty}^{\infty}\beta_0(t_0)\cdot\sin(\omega\cdot t)e^{i\cdot\omega_0\cdot t_0}\cdot dt_0 \tag{2.35}$$

Finally, the time-dependence of β_0 should be similar to that demonstrated in Figure 1. That Figure shows a snapshot of velocities – how velocity changes with coordinate z for a given time. A single electron sees this pulse passing through the electron's position as time goes by. Thus, a good approximation of time-dependence for β_0 would be a Gaussian with time constant τ, the duration of the pulse:

$$\beta_0(t)=\beta_{\max}\cdot e^{-\frac{t^2}{\tau^2}} \tag{2.36}$$

Plugging this into the formula for $F(\omega)$ gives us our final integral:

$$F(\omega)=\frac{\beta_{\max}}{2\cdot\sqrt{2\cdot\pi}}\cdot\int_{-\infty}^{\infty}\exp\left(-\frac{t_0^2}{\tau^2}+i\cdot\omega\cdot t_0\right)\cdot\left(\exp(i\cdot\omega\cdot t_0)-\exp(-i\cdot\omega\cdot t_0)\right)\cdot dt_0 \tag{2.37}$$

Here we wrote out sine as a sum of two complex exponents. If ξ_1 and ξ_2 are given by:

$$\begin{aligned}\xi_1&=\frac{t_0}{\tau}-\frac{i\cdot(\omega_0+\omega)\cdot\tau}{2}\\ \xi_2&=\frac{t_0}{\tau}-\frac{i\cdot(\omega_0-\omega)\cdot\tau}{2}\end{aligned} \tag{2.38}$$

Then main integral can be rewritten as:

$$F(\omega)=\frac{\beta_{\max}}{2\cdot\sqrt{2}\cdot\pi}\cdot\left[\int_{-\infty}^{\infty}\exp\left(-\frac{t_0^2}{\tau^2}+i\cdot(\omega_0+\omega)\cdot t_0\right)dt_0+\int_{-\infty}^{\infty}\exp\left(-\frac{t_0^2}{\tau^2}+i\cdot(\omega_0-\omega)\cdot t_0\right)dt_0\right]=$$

$$=\frac{\beta_{\max}}{2\cdot\sqrt{2}\cdot\pi}\cdot e^{-\left[\tau\cdot\frac{\omega_0+\omega}{2}\right]^2}\cdot\int_{-\infty}^{\infty}\exp\left(-\xi_1^2\right)\cdot d\xi_1+\frac{\beta_{\max}}{2\cdot\sqrt{2}\cdot\pi}\cdot e^{-\left[\tau\cdot\frac{\omega_0-\omega}{2}\right]^2}\cdot\int_{-\infty}^{\infty}\exp\left(-\xi_2^2\right)\cdot d\xi_2=$$

$$=\frac{\beta_{\max}\cdot\tau}{2\cdot\sqrt{2}}\cdot\left[e^{-\left[\tau\cdot\frac{\omega_0+\omega}{2}\right]^2}+e^{-\left[\tau\cdot\frac{\omega_0-\omega}{2}\right]^2}\right]$$

(2.39)

This is the final result that describes the energy spectrum of the broadband radiation detected. To summarize, the full spectrum of the radiation consists of the following components: first, radiation at the incoming light's frequency ω - because of the circular motion of electrons; second, radiation at multiples of the incoming light's frequency - because an observer sees the charges moving in circles but with non-uniform speed because of retardation effects; third, the broadband radiation with frequency dependence $F(\omega)$ - because driving pulse makes the electron orbit unstable, incurring Gaussian time dependence of the electron's velocity.

The frequency at which we observe the radiation has been deliberately chosen not to be a multiple of the incoming light's frequency. This was done to minimize the contribution to the signal detected from the frequency multiplying effects of the plasma on the incoming laser light. Depending on the electron's speed in the *z* direction, up to all three components might contribute to the synchrotron radiation detected.

When synchrotron radiation is created by electrons that do not move along the beam path (*z* axis) only the third component contributes to the result measured. Moving electrons "see" the laser light at wavelength $800nm$, making contributions from the first

two components irrelevant. Another case is when the electrons have some velocity along the z axis – this changes the wavelength of the driving light as felt by the moving electron. Thus radiation due to the second component above would be detected. Finally, if electrons are really relativistic ($\gamma = 3/8$ or $\beta = .927$), they would see the driving laser light as having a wavelength of $300nm$. This would result in the first component mentioned above as the source of the radiation detected.

The main contributions to the synchrotron radiation detected are thought to be components two and three, however, because of the low probability electrons becoming highly relativistic in the z-direction.

Once again, let's consider linearly polarized laser light. As noted in the end of section 2.1, electrons in that case would exhibit somewhat similar orbits. Furthermore most of the discussion above is applicable to a linear polarization case. The only difference is that instead of the circle we now have a figure ∞ as an orbit for the radiating electron. The trajectory of the electron is described a little differently, namely, the y-component has twice the period it had before. Thus (2.22) turns from this form:

$$\begin{aligned} &\vec{n} = (1,0,0) \\ &\vec{\beta} = \beta_0 \cdot (\cos(\omega \cdot t), \sin(\omega \cdot t), 0) \\ &\frac{d}{dt}\vec{\beta} = \beta_0 \cdot \omega \cdot (-\sin(\omega \cdot t), \cos(\omega \cdot t), 0) \end{aligned} \tag{2.22}$$

Into:

$$\vec{n} = (1,0,0)$$

$$\vec{\beta} = \beta_0 \cdot b \cdot \left(\cos(\omega \cdot t), a \cdot \sin(\frac{1}{2} \cdot \omega \cdot t), 0 \right) \tag{2.22a}$$

$$\frac{d}{dt}\vec{\beta} = \beta_0 \cdot \omega \cdot b \cdot \left(-\sin(\omega \cdot t), a \cdot \frac{1}{2} \cdot \cos(\frac{1}{2} \cdot \omega \cdot t), 0 \right)$$

Note the constants a and b in the formulas – those are introduced to make up for the difference between the figure ∞ and the circular trajectory. Furthermore, constant a describes the difference in strength between the Coulomb and Lorenz forces that electron feels.

Propagating this difference all the way down to the answer will affect the result slightly. The leading power in the exponential integrals above is due to the Gaussian shape of the pulse. This makes our integral in the form of $\exp(-x^2)$. The electron's trajectory contributes by adding the first order into the exponent: $\exp(-x^2 + a \cdot x)$, where a is some constant. Thus substituting (2.22a) for (2.22) will alter the whole calculation only slightly. Namely, the constants in front of the frequency-dependent terms would change a little bit.

The qualitative discussion above could be summarized as follows: laser driven electrons radiate broadband radiation regardless of the polarization of incident light.

2.3. Radiation of multiple charges, moving coherently

Now we are ready to calculate interference from all of the moving charges. Let's consider radiation from two charges. An important quantity to know is the phase

difference between the radiations coming from the two charges. There are two terms in this phase difference. The first term is due to the fact that charge that is "upstream" is accelerated earlier:

$$\Delta\phi_1 = 2\cdot\pi\cdot\frac{z}{\lambda} \tag{2.40}$$

The second term is a typical interference phase difference. Imagine two rays which are distance z apart and at an angle Θ with the x axis. The path difference is then $z\cdot\sin(\Theta)$. Thus the phase difference is:

$$\Delta\phi_2 = 2\cdot\pi\cdot\frac{z\cdot\Theta}{\lambda_{out}} \tag{2.41}$$

Here λ_{out} is the wavelength at which we measure intensity. Also, a small-angle approximation for sine has been made. The contribution of a single charge would then be:

$$dE = E(z,t)\cdot\cos(\Delta\phi_1 + \Delta\phi_2) \tag{2.42}$$

Where $E(z,t)$ is given by formulas (2.23) and (2.16). To unite everything in one formula:

$$dE = \exp\left[-\left(\frac{z-z_0}{a}\right)^2\right]\cdot\frac{\beta_0 - \cos(\omega\cdot t - z\cdot k)}{(1-\beta_0\cdot\cos(\omega\cdot t - z\cdot k))^3}\cdot\cos\left[2\cdot\pi\cdot z\cdot\left(\frac{1}{\lambda}+\frac{\Theta}{\lambda_{out}}\right)\right] \tag{2.43}$$

An extra term has been added – to account for the fact that pulse is a Gaussian centered around z_0. The size constant of this Gaussian is a. Integrating this over all possible values of z for fixed time gives us the angular distribution of radiation.

To the first order, the effect modeled here and shown in Figure 3 is the constructive interference of $N = 50$ sources. When the detector is in the point in space where light from the sources interferes constructively, electric fields produced by each source at the detector are added. The measured light's intensity, however, is proportional to the square of the electric field. Thus if N turns of spiral produce interfering light, the resultant intensity goes as N^2. Figure 3 shows the results of a calculation finding intensity as a function of angle at which we observe the radiation. The angular Full Width Half maximum (FWHM) of radiation emitted is $3mrad$.

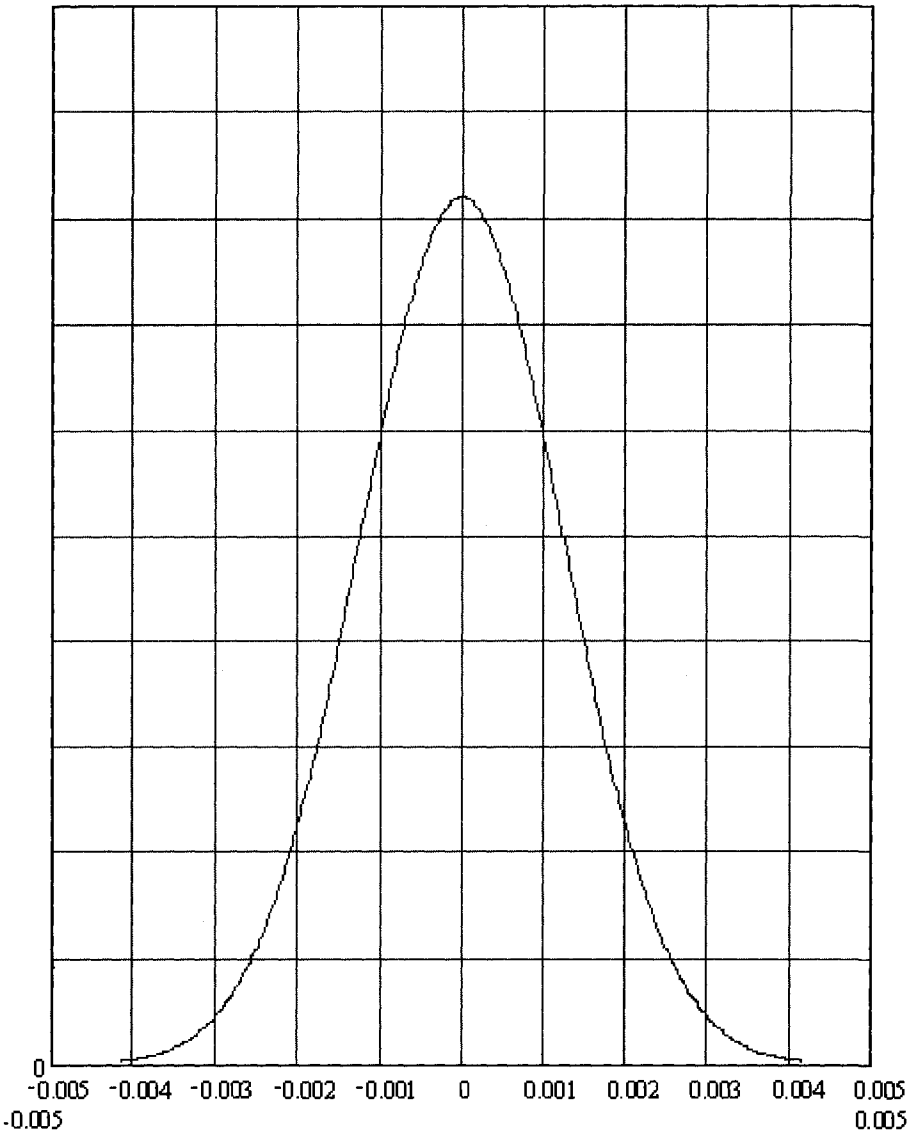

Figure 3. Intensity (abs units) of the light radiated vs. angle of observation (rad) in the horizontal plane.

2.4. Number of coherent electrons needed to create observable radiation

All the considerations presented above indicate that there will be broadband synchrotron radiation emitted by electrons in the focal point. Before proceeding on to the experimental part one needs to figure out whether this radiation is detectable at all. The computations below repeat one presented by Kaplan and Shkolnikov in (2002).

Following the discussion by Garret in (2002) one could find that an electron rotating at the laser frequency ω_0 will then emit synchrotron radiation, with a frequency cutoff given by:

$$\omega_{\max} \approx 3\gamma^3 \omega_0 \tag{2.44}$$

For the specific parameters of this experiment one finds from 2.44 and calculation behind Figure 2 ($\lambda = 800nm$, $\gamma \approx 3$) that the cutoff of the synchrotron emission occurs at $155eV$, with the strongest emission in the $15eV$ to $30eV$ range (10%-20% of I_{max} [10]).

Following the procedure in [2], we can find that for experiments with the USP laser, the photon bursts should be detectable if the electrons radiating are coherent. For example, in a plasma with an electron density equal to $10^{21} cm^{-3}$, the focal volume should contain about $N=10^{10}$ electrons. If each of these electrons were radiating independently, one would expect only a single $15eV$ photon to be radiated per burst. However, if the photons can radiate coherently, the power scales as N^2 instead of N, raising the output by a factor of 10^{10}! While this fully coherent case would be easily detectable, the total power radiated ($2.5GW$) would still remain much less than the driving laser power ($10TW$), so the calculation of the radiation back-reaction on the electrons is not critical.

To summarize, forcing electrons to radiate synchrotron radiation of sufficient energy to be detectable is theoretically possible. Calculations above indicate that electrons will move in a way making broadband radiation possible. Furthermore, interference phenomena would shape the outgoing radiation. Finally, enough electrons are thought to participate in the process to make it feasible to detect the output. Measures to create, filter, and detect synchrotron radiation are discussed in the next chapter.

3.0. EXPERIMENTAL SETUP

In this chapter, we present a general overview of all of the experimental procedures. The experimental setup, laser targeting, and focusing techniques are presented. Laser polarization and shot-to-shot energy variations are also discussed.

3.1. General description of the experiment

The goal of the experiment is to look for the synchrotron radiation from laser-plasma interaction. To achieve this we focused a circularly polarized laser beam on a metal target. Focusing has been done in the vacuum to prevent self-focusing and self-guiding effects due to the interaction of intense laser light ($I = 10^{19} W/cm^2$) and air. This intense laser light drove electrons to create the synchrotron radiation. A lens was used to collimate this radiation before it left the experimental chamber. Finally, a diffraction grating and filter were used to limit the wavelength of light hitting our CCD to $300nm$.

For testing and alignment shots, flat plane aluminum targets were used. For data shots, $18\mu m$ tungsten wire was used. Data from shots with linearly and circularly polarized light were recorded and compared.

There are four components in the experimental setup. Table 1 describes those components:

Table 1. Elements of the experimental setup.

Component	**Consisting of**	**Pressure needed for operation**
Ultra Short Pulse laser	Seed laser, Amplifiers	Atmospheric
Compressing and Polarizing	Compression gratings, Purely reflective circular polarizer	microTorr
Experimental Chamber	Flat mirrors (2) Off-axis parabolic mirror Target mounted on 3D micro movement stage Collimating lens	microTorr
Detection and Noise elimination	Filtering window on the experimental chamber Diffraction graging Filter on the CCD CCD	Atmospheric

The first phase provides us with the laser pulse itself. As with all tabletop Ultra Short Pulse lasers, we start with the seed amplifier that gives out a short pulse ($100\,fs$ duration, few nanoJoules per pulse). The pulse is stretched to several hundred

picoseconds duration with a pair of diffraction gratings. A series of amplifiers adds energy to the pulse. Pockel cells, among other devices, are used to cut out some of the Amplified Spontaneous Emission Prepulse. All of the amplifiers use Ti: Sapphire crystal for the lasing medium. The lasing transition for the crystal corresponds to light with a wavelength near $800nm$, with a large ($\sim 30nm$) bandwidth. Leaving the first phase, the pulse is still spatially stretched. Thus energy density never reaches air's ionization point so all the manipulations could be done at atmospheric pressure.

The second phase starts with the beam entering the vacuum chamber. Two diffraction gratings compress the pulse. Now, after compression, the energy density reaches $10^{16} J/m^3$. This corresponds to electric fields on the order of $10^{13} V/m$. That's why we need a vacuum (microTorr pressures) from this point until we hit the target – air would break down into plasma well below the energies we have now. The compression gratings work only on linearly polarized light, so the natural position of the circular polarizer is right before the experimental chamber. We have extremely high energy light to circularly polarize. For the intensities cited, transmission optics will distort and disperse the short pulse. Thus, making the beam to be circularly polarized is a challenge: a purely reflective system is needed. This system was created with a system of seven large, specially-coated mirrors, most with a high angle of incidence.

To understand how the system works we need to introduce more terminology. There are two principle directions describing the direction of polarization of light incident on the surface of the mirror. "S" polarization is parallel to the surface of the mirror while the "P" direction is perpendicular to the $\vec{k}$ -vector of the light. Components of the

electric field directed along those two directions experience different changes during reflection from any surface (exact quantitive discussion involves boundary condition consideration and was presented by Jackson (1998)). Furthermore, coatings on the seven mirrors are birefringent, so "S" and "P" components accrue different delays as they travel through the system. Thus, the net relative phase change adds up to be ninety degrees, which means that light changes its polarization from linear to circular. For the linearly polarized light we bypass this system. For circularly polarized light, we send it through the system.

The third phase also happens at microTorr pressures. We transmit our beam into the experimental chamber with help of five mirrors. Then, we focus it with a $2.5cm$ diameter, off-axis parabola. Our targeting procedure ensured that the target is positioned in the laser focus. The emitted radiation should be at a right angle with the incident beam, so a corresponding window is positioned accordingly. Between the window and the target we added a collimating lens. The focus of the lens is $10cm$, which is the distance between the target and the lens. Thus the lens effectively maps the angle of the outgoing radiation onto linear displacement (both horizontal and vertical). Figure 4 is a schematic drawing of the experimental chamber.

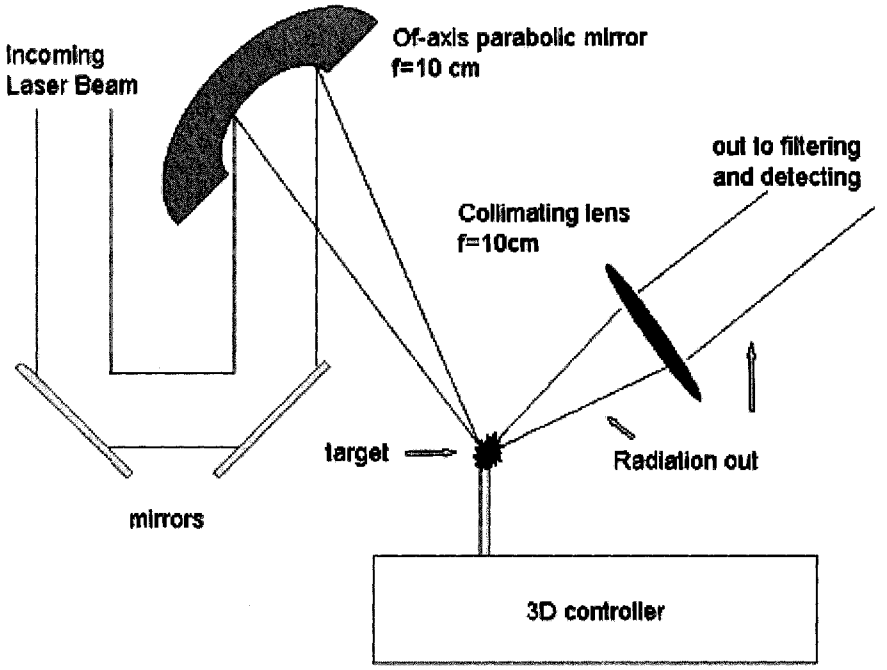

Figure 4. Experimental chamber (top view).

The fourth phase is data filtering and acquisition. The purpose of the experiment is to measure synchrotron radiation from laser driven electrons. This means that our filtering system should filter radiation from all other processes. One of those processes is frequency multiplication of incoming laser light due to plasma-light interaction. Thus the detection wavelength was deliberately chosen not to be an integral divisor of $800nm$. Another restriction on the wavelength detected was the transmission of the glass in the experimental chamber's window. This glass doesn't transmit much of the radiation with wavelengths below $270nm$.

All the considerations above led us to choose $\lambda = 300nm$ as the detection wavelength. Filtering was done by a diffraction grating and interference filter. The interference filter was placed directly above the CCD shutter. The diffraction grating was positioned in such a way as to direct the first order maximum downward onto the CCD for $\lambda = 300nm$. This positioning requirement means that the grooves of the grating should be horizontal. Figure 5 shows the data filter and acquisition part of the experiment. The chamber's window cuts out short wavelengths (below $270nm$) while the grating and filter isolate a small bandwidth around $300nm$ to go into the CCD.

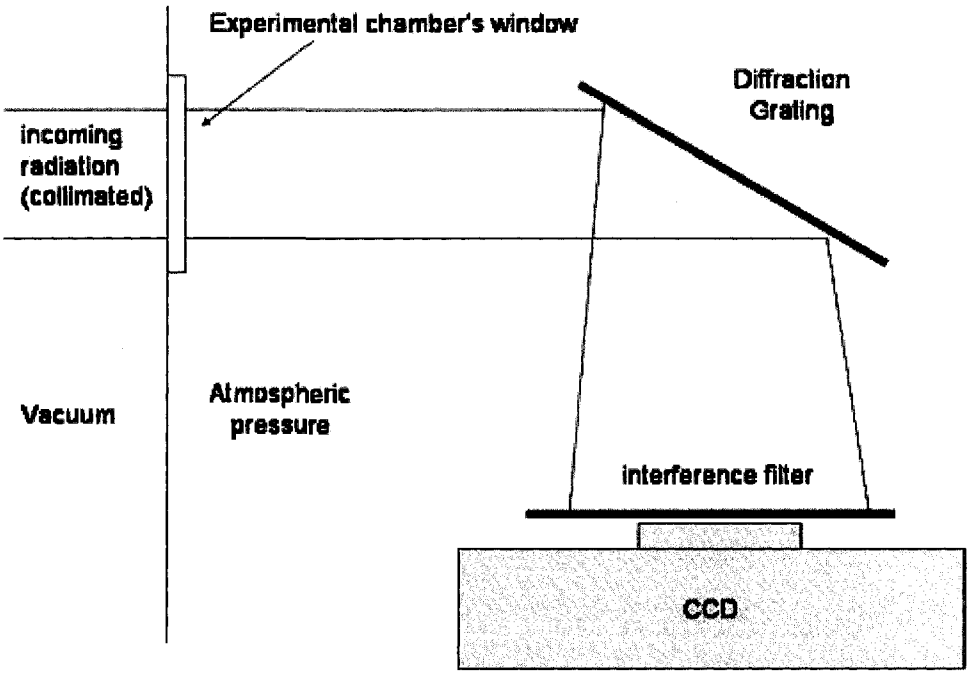

Figure 5. Data filtering and acquisition (side view).

3.2. Measuring light's polarization

The experiment requires circularly polarized laser light. The idea was to contrast results from circularly and linearly polarized light. However, a USP laser (like any other laser) produces linearly polarized light. The seven mirror, purely reflective system was implemented to attempt to circularly polarize light (see section 3.1). Thus, we needed to measure the polarization of the beam as it enters the experimental chamber. The principal set up is shown in Figure 6.

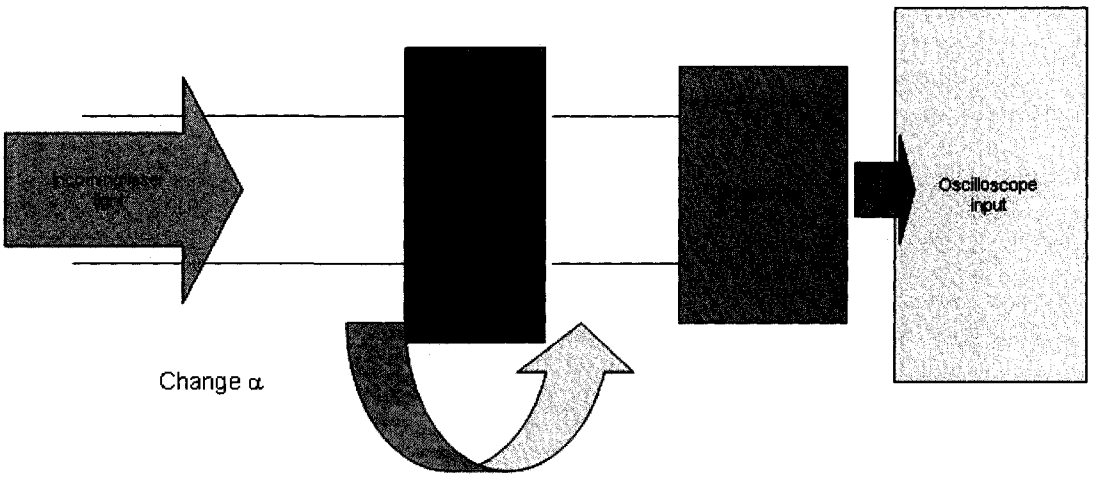

Figure 6. Principal set-up for measurement of polarization.

The angle between the polarizer's maximum transmission and some fixed axis is α. Changing α and measuring the intensity of the electric field one can gauge the polarization of the light. Graphing the intensity of the light that reaches photodiode will give us an idea of how the light is polarized. The photodiode's output is fed into the oscilloscope. The incoming laser was set into low energy $10Hz$ pulse mode. For a given α, an average of 20 pulses would be displayed on the oscilloscope. Another recorded quantity is the maximum deviation of the diode's output for the 20 pulses. The results are presented after the exact calculation of what we were measuring: the intensity of the light that is transmitted through the polarizer to the diode.

Basic considerations tell us that for circularly polarized light, the polarizer's angle shouldn't affect the intensity. The safer assumption to make, however, is that incoming light is polarized elliptically. Let's chose our coordinates x and y in such a way that the major axis of the ellipse is along the x axis and the minor axis of the ellipse is along the y axis. The x and y components of the electric field are then:

$$\begin{aligned} E_x &= E_{0x} \cdot \cos(\omega \cdot t) \\ E_y &= E_{0y} \cdot \sin(\omega \cdot t) \end{aligned} \tag{3.1}$$

Here we set the zero time moment to when the electric field is aligned along the x axis. If α is the angle between the polarizer and the x axis then the electric field along the polarizer is

$$E = E_x \cdot \cos(\alpha) + E_y \cdot \sin(\alpha) = E_{0x} \cdot \cos(\omega \cdot t) \cdot \cos(\alpha) + E_{0y} \cdot \sin(\omega \cdot t) \cdot \sin(\alpha) \tag{3.2}$$

This is the electric field that is transmitted through the polarizer to the diode. The diode measures the intensity of the light, which is proportional to the time-average of the square of the electric field. First, let's square E:

$$E^2 = E_{0x}^2 \cdot (\cos(\omega \cdot t) \cdot \cos(\alpha))^2 + E_{0y}^2 \cdot (\sin(\omega \cdot t) \cdot \sin(\alpha))^2 + \\ + 2 \cdot E_{0x} \cdot E_{0y} \cdot \cos(\omega \cdot t) \cdot \sin(\omega \cdot t) \cdot \cos(\alpha) \cdot \sin(\alpha) \tag{3.3}$$

Now, we need to remember that basic trigonometry gives us:

$$(\cos(\omega \cdot t))^2 = \frac{1}{2} + \frac{1}{2} \cdot \cos(2 \cdot \omega \cdot t)$$
$$(\sin(\omega \cdot t))^2 = \frac{1}{2} - \frac{1}{2} \cdot \cos(2 \cdot \omega \cdot t) \tag{3.4}$$
$$2 \cdot \sin(\omega \cdot t) \cdot \cos(\omega \cdot t) = \sin(2 \cdot \omega \cdot t)$$

But the time averages of $\sin(2 \cdot \omega \cdot t)$ and $\cos(2 \cdot \omega \cdot t)$ are zero. Thus the time average of square of the electric field is:

$$E^2 = E_{0x}^2 \cdot \frac{1}{2} \cdot (\cos(\alpha))^2 + E_{0y}^2 \cdot \frac{1}{2} \cdot (\sin(\alpha))^2 = E_{0x}^2 \cdot \frac{1}{2} \cdot (\cos(\alpha))^2 + E_{0y}^2 \cdot \frac{1}{2} \cdot \left(1 - (\cos(\alpha))^2\right) = \\ = E_{0y}^2 \cdot \frac{1}{2} + \left(E_{0x}^2 - E_{0y}^2\right) \cdot \frac{1}{2} \cdot (\cos(\alpha))^2 = E_{0y}^2 \cdot \frac{1}{2} + \left(E_{0x}^2 - E_{0y}^2\right) \cdot \frac{1}{2} \cdot (1 - \cos(2 \cdot \alpha)) = \\ = \frac{1}{4} \cdot \left(E_{0x}^2 + E_{0y}^2\right) + \frac{1}{4} \cdot \left(E_{0x}^2 - E_{0y}^2\right) \cdot \cos(2 \cdot \alpha) \tag{3.5}$$

Thus we can predict the following: The signal has to be periodic with a period of 180 degrees in angle of the polarizer - α. The ratio of maximum to minimum intensity should be:

$$\frac{\max(I)}{\min(I)} = \frac{E_{ox}^2}{E_{oy}^2} \tag{3.6}$$

Maximum intensity occurs when cosine in the formula is +1 and minimum intensity corresponds to cosine equals -1. We are interested in the ratio of the fields'

components, not the intensities. So the final measure of the ellipticity of our polarization would be the square root of the ratio maximum and minimum intensities.

Figure 7 shows intensity (which is proportional to the voltage from the photodiode used to detect light) as a function of α :

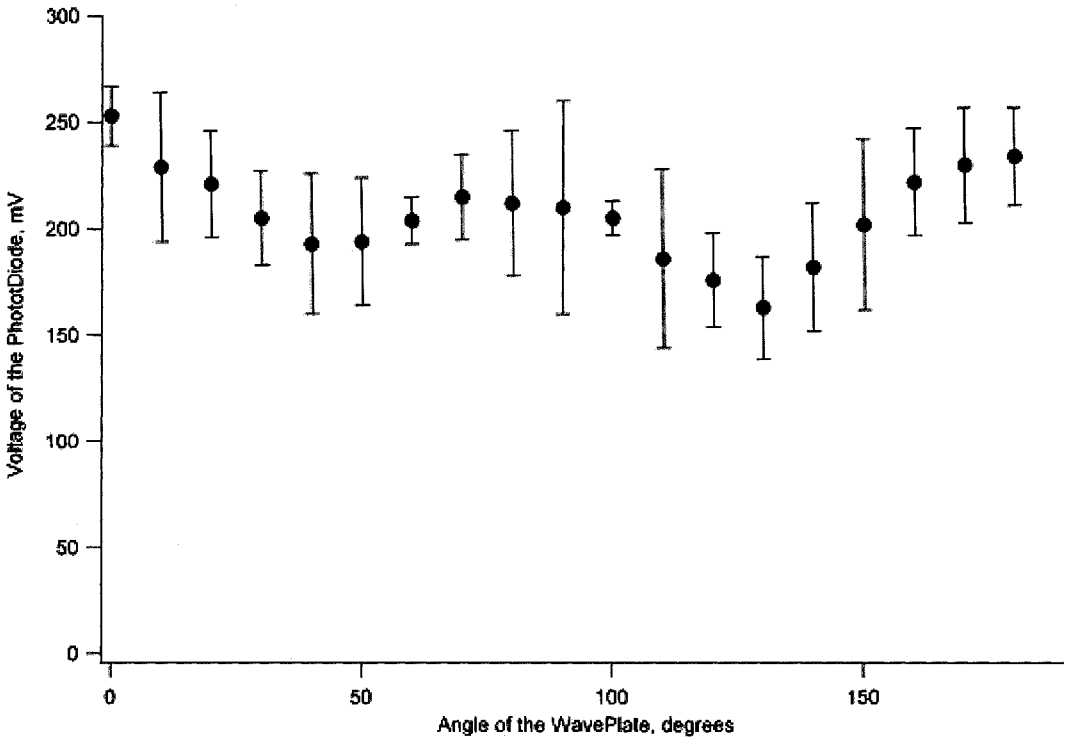

Figure 7. Intensity of the light versus angle of the wave plate.

One could clearly see that the conclusions presented above are correct. It might be safe to assume that the light measured is elliptically polarized. The max/min ratio for intensity is 1.2. Thus the end of the vector describing the electric field travels in an ellipse with a ratio of ~1.1 for major/minor axes. Within ten percent accuracy our light is circularly polarized. In conclusion, let me restate the results of the polarization measurement: The seven mirror purely reflective circular polarizer works: light is

elliptically polarized after it. The major/minor axis ratio of the E-field ellipse is around 1.1.

Another noteworthy observation is that the maximum deviation for the intensity for a given angle stays roughly the same throughout the table. This deviation is mainly due to the fluctuation of the laser's power itself.

3.3. Low power shots energy statistic

At low energy and in ten-pulse-per-second mode, the laser's output could vary significantly from shot to shot. However, the energies seem to be scattered around some average value. In other words, for a number of 20-shots series, one observes almost the same average in each series while registering significant standard (or maximum) deviation. Table 2 represents one hundred consecutive low power shots:

Table 2. Energy of the pulse for 100 consecutive low-power shots

49	52	48	50	48	49	48	44	49	41
42	47	47	49	47	46	48	46	49	46
45	49	47	46	48	51	42	44	46	45
51	46	48	46	50	48	48	46	45	45
44	45	48	44	46	47	46	46	48	46
47	45	46	48	44	49	48	41	47	50
47	41	47	45	48	48	48	45	43	42
48	0	48	46	46	47	47	48	49	45
48	47	49	50	45	42	42	49	48	49
47	46	50	43	47	48	49	50	49	47

Elementary statistical analysis gives an average of 46.3 and a standard deviation of 5.2. This big scatter in energy for different shots should not concern us, however. The main experiment is conducted in single shot mode: one CCD scan per shot.

There are two reasons not to record radiation from repetitive shots on the same CCD scan. First, the target doesn't stay in one place (and in the case of the wire is destroyed). During the repetitive shots it receives some kinetic energy after each successive shot. On top of that, acoustical vibrations due to the machinery in the laboratory always make the target oscillate. Second, such repetitive shots would need to be done with a solid metal target. The first shot would make a crater on the metal's surface. Each successive shot would deepen the crater, thus moving the metal's surface further and further from the focus of the beam.

3.4. Beam focusing

The idea is to focus the beam to as small of a spot as possible. There are several limiting factors on how small the focal spot could be. One of those factors is the diffraction limit – photons still have to obey Heisenberg's uncertainty principle, so we cannot know their transverse coordinate with perfect accuracy. Another factor is that laser beams are described by a cylindrically symmetric solution to Maxwell equations which imply a minimal width of the beam beyond which the beam cannot be focused. (Both restrictions have the same mathematical basis – looking for a wave solution to the

Laplace's equation. The limitation due to the Heisenberg's principle is significantly more restrictive, and is ignored in further considerations.)

On top of the limiting factors that are enumerated above focusing optics itself might result in an unsatisfactory big focal spot. A parabolic mirror was chosen because geometrically, a parabola is the only shape that can focus a collimated beam to a point (here we consider only geometrical optics, which disregards the limitations discussed above).

With the parabolic mirror focusing the beam, we are limited only by the properties of the laser beams. The laser beam (Gaussian $E_{0,0}$ mode) could be conveniently described by two parameters, w_0 and z_0. (There is really just one free parameter; w_0 and z_0 are related through wavelength as shown in (2.16).) If we are at the focus of the beam, w_0 is how far we need to move radially (in the direction perpendicular to k-vector of the wave) to lower the intensity of the beam by a factor of $1/e^2$. It is convenient to think of as w_0 the "waist size" of the beam. The parameter z_0 denotes how far downstream of the focus we need to move to lower the intensity by a half. The general formula is:

$$E(r,z) = E_{\max} \cdot e^{-\left(\frac{r}{w_0}\right)^2} \cdot \frac{1}{\sqrt{1+\left(\frac{z}{z_0}\right)^2}} \tag{3.7}$$

From that formula one can show that the laser beam (for distances much bigger then z_0) diverges at the angle:

$$\theta = \frac{\lambda}{w_0 \cdot \pi} \tag{3.8}$$

Our mirror has a focal distance $f = 10cm$. If our beam has diameter $d = 2cm$ we can derive an equation for w_0:

$$\frac{\lambda}{w_0 \cdot \pi} = \theta = \frac{d}{2 \cdot f}$$

$$w_0 = \frac{\lambda \cdot 2 \cdot f}{d \cdot \pi} \approx 2.46 microns \tag{3.9}$$

One could derive conversion coefficient to go from w_0 to full width half-max (FWHM) diameter. It is a number around 1.19. Thus theoretical lower limit on FWHM is $2.93 \mu m$.

Focusing is done at atmospheric pressure since it requires manual mirror alignment (for both straight mirrors and the parabolic one). The focusing process needs to be observed in real time. To achieve that we used a microscope attached to a camera. That camera was connected to the monitor. When the microscope had focus at its focal spot we needed to attenuate the signal in order not to burn the camera. A series of filters with combined optical densities (ODs) of up to 10 was used. In addition, most of the amplifiers were disabled for the focusing.

Once we focused the beam we needed to measure its size. A frame-grabber card captured the camera image onto a computer file. The microscope-camera-computer system was calibrated on the standard NAVY micro-target reticle (.8 microns per pixel was the resulting scale). Thus once we acquired data the measurement turned into simple

pixel counting. The spot size for our focus was measured to be between 4 and 5 microns FHWM.

3.5. Rough targeting and target holder

Once the focusing phase was complete, we needed to position our target at the focus of the beam. Fortunately, our microscope/camera were still focused on the focal point of the beam. Thus placing the wire so it was visible with the microscope would put the wire at around the point needed.

Two telescopes outside of the chamber were focused on the target. Now we could move target around: if it remained clearly visible on both telescopes it had to be near the focus. Both telescopes were attached to the cameras and their own monitors. This enabled us to mark the initial position of the wire on the telescopes' monitors for double-checking. One telescope with position marked on the monitor or two telescopes at an angle to one other should be enough. The redundancy is used to increase precision in target positioning.

All three monitors (the microscope's and both telescopes') would show the wire at this stage of the alignment. Now we had a way to repeatedly put the target in and out of focus. This is very useful, since our target holder holds 14 wires, so we wouldn't have to vent and repeat targeting after each shot. The target holder and the wires are shown in Figure 8:

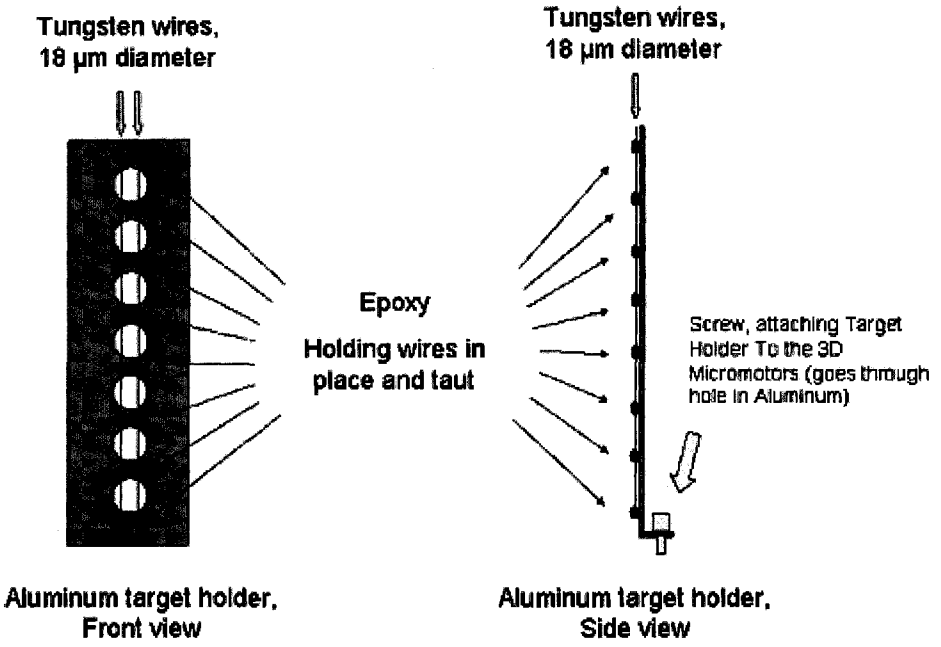

Figure 8. Target holder and the Tungsten wires.

To summarize rough targeting procedures: Rough targeting is done at atmospheric pressure. We use the microscope and the two telescopes. All devices have cameras mounted on them. The cameras display the process live on the monitors. The microscope is used to focus the beam and position the wire at the focus of the beam. Then, the telescopes are focused on the wire to pinpoint the position. Also, the wire's position on the monitors is marked. After that the telescopes are not moved throughout the experiment (until the next vent).

3.6. Data acquisition and system alignment

We need to align the diffraction collimating lens and grating so $300nm$ light is reflected onto the CCD chip. By now, our telescopes point to the focus, so the target holder and the microscope are taken out. A low-energy ($30-70mJ$ per shot) repeating ($10Hz$) pulse is introduced into the experimental chamber. At the focus, air breaks down into plasma since all the energy is tightly focused in the small spot. The repetitive spark thus produced radiates visible light in all directions. This visible light is used to ensure that the collimating lens is positioned correctly, i.e light after the lens is a steady, collimated beam.

The next step is to manually adjust the grating. There are two goals: all collimated radiation must hit the grating and the first order maximum reflection from the grating must hit the CCD chip (for $300nm$). A two-part mounting system for the grating is implemented. The grating is mounted on a 3D movement stage (three screws tilt the plate that the grating is mounted on). The stage itself is mounted on the outside wall of the chamber. This mounting occurs through series of rods and holds. The way the stage is mounted is adjusted so the entire collimated beam hits the grating. Then the 3D stage is moved so the grating reflects $300nm$ radiation onto CCD.The $300nm$ light is not visible (it is UV). However, deep violet ($400nm$) and green ($550nm$) are visible. Thus, one can gauge where $300nm$ radiation reflected off the grating would end up.

Now we are ready to take CCD scans of 30 repetitive sparks. We set the CCD time scan for 3 sec (with the spark frequency still at $10Hz$) and do a scan. Results are

displayed on the computer screen. Then we move the grating (using the 3D stage) to maximize the intensity of the radiation hitting the CCD's chip. Also, we try to center the picture on the computer. The spark radiates in all directions. This means that light from the spark fills the CCD in both up-down and left-right directions. This light is not of uniform intensity. As one moves away from the perfect alignment the intensity drops off. Centering the picture provides a means of fine-tuning the alignment of the whole data acquisition system. Once that is achieved, the target is put back into place: we then pump down the target chamber to microTorr pressure.

There is one last grating alignment that needs to be done because the pump down often shifts the chamber slightly. The aluminum target holder is put into the focus. A series of 30 low energy ($70mJ$) shots is fired at the metal at vacuum. Radiation from that is scanned by the CCD. Once again, grating is adjusted to maximize intensity of the light hitting the CCD's chip and to center the picture displayed.

The steps described above proved to be sufficient to ensure that the $300nm$ radiation emitted from the focus of the laser beam got to the CCD.

3.7. Fine targeting at microTorr pressures

There are two types of targets: aluminum metal for alignment and tungsten wire for data acquisition. To do targeting for both we need to reduce the energy per shot so we don't damage the targets and targeting optics. Thus low level repetitive light hits the target. Light reflected off the target is displayed on the telescopes' monitor. For

aluminum, fine targeting is easy: move the target to minimize the size of the reflected light spot on the monitor.

For tungsten wire fine targeting is trickier. The 3D micro motor stage has two motors moving the target in the horizontal plane. One motor (we called that coordinate *w*) moves the target up or down stream (along the original pulse's k-vector). Another motor (coordinate *x*) moves the target at an angle to the first one. For a given *w* we would find the range of *x* for which reflected light is still visible. Then we would find *w* for which that range is minimal. Then we would adjust *x* to maximize the brightness of the reflected spot. See Figure 9 for more geometrical details.

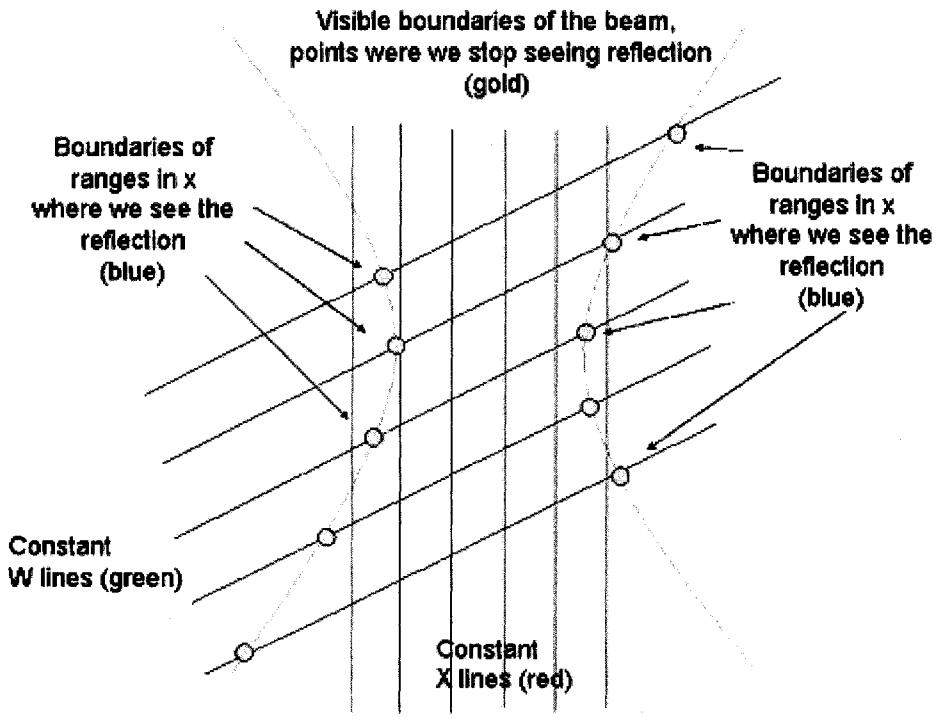

Figure 9. Moving target in and out of focus.

When we fix w and change x, the target moves along a green line. We record values of x corresponding to the blue circles on that green line. We find w for which that range is minimal. Then changing x we go to the middle of the line.

Understanding what really affects the intensity of the reflected light is quite challenging. The wire (18 micron diameter) is bigger then the focus (around 4 microns) and circular. Radiation emitted might have complicated phase profiles. However, data taken suggests that our basic assumptions are correct:

For aluminum, the smallest and brightest reflections indicate the best target positioning. For tungsten, the small range in x for which we see the reflection means we are near the focus. Another sign of good target placement is the brightness of the reflections.

The experimental setup presented above is geared towards the production of the broadband synchrotron radiation. The decision to use thin ($18\mu m$) tungsten wire as the target was made in an attempt to minimize noise through reducing the total amount of material involved (ablation craters on metal are usually on the order of$100\mu m$. This means that in our case we had at least 10 times less of the material, giving some credence to the hopes of having compact small plasma interacting with the laser beam). The radiation detection wavelength was chosen to allow us to study synchrotron radiation exclusively. Those and many other considerations allowed us to successfully detect synchrotron radiation from laser driven electrons in the plasma.

4.0. EXPERIMENTAL RESULTS

In this chapter experimental data is presented, analyzed and discussed. The fact that we are able to detect anything at all is due to the fact that a sufficient number of the electrons is moving coherently. The angular distribution of the outgoing radiation allows us to estimate the spatial coherence length for the movement of the electrons. Light detected by the CCD is a result of constructive interference of all those electrons that move coherently.

As discussed in section (2.1), each electron emits a cone of light along its velocity as it spins around in a circle. The position of a single electron in its orbit is determined by the direction of the electric field of the driving laser light. Our radiating structure consists of a collection of those electrons (at different phases in the circle as we move along the beam). Furthermore, the length of this structure is on the order of 50 wavelengths of the driving light – thus the radiating spiral has around 50 turns. This spiral moves like a barbershop spiral, rotating at the laser frequency. Light radiated by this spiral is a result of the interference between light emitted by all the individual electrons.

All the electrons radiate in the directions tangential to their movement. The radii of their orbits are very small (around a micron), so from the outside it looks like the radiation comes from the center of the spiral. This light is collimated by a lens that is placed its focal distance away from the spiral.

Lens placement insures that the left-right axis on the CCD maps to the angle in the horizontal plane for the radiation. The up-down axis on the CCD maps to the wavelength of the radiation (because of the diffraction grating) convoluted with the emission angle in the vertical plane.

One of our goals is to prove that there is sizeable spatial coherence in the movement of the laser driven electrons. The smaller the angle discussed above the longer the spatial coherence of the radiating electrons.

4.1. CCD output

The data collection was done by a CCD (SpectraSource Instruments HPC-1). The CCD detects light using $1cm^2$ silicon chip which is divided into 262,144 (512 by 512) pixels. In the chip, incoming photons are converted into electrons with the number of electrons proportional to the incoming photon's energy. Thus, the CCD's output is a 512 by 512 matrix of positive integer numbers. Each number is proportional to the total light intensity at the particular pixel of the CCD chip.

The CCD was hooked up to the computer utilizing the NIH imaging program. Data from this program was converted into an ASCII text file for further analysis with the help of the Igor data analyzer. Due to the memory size limitations of the analysis program each CCD image had to be cut in half. Only halves that include image are presented here.

As described in Chapter 3, the lens collimates emitted radiation. This maps the angle in the horizontal plane onto a left-right position on the CCD. (The diffraction grating groves are horizontal, so this grating doesn't affect the left-right mapping). This setup allows us to easily see the angular spread of the radiation in the horizontal plane. This spread that is limited by the interference of the spiral of radiating electrons. This narrow spread should be represented by a narrow vertical stripe on the CCD image.

The up-down axis on the CDD is more complicated. The result is a convolution of two effects. First, the lens maps angle with horizontal axis onto the up-down position. Second, the diffraction grating disperses light according to its wavelength. Finally, the filter sharply attenuates all light that is not around $300nm$ in wavelength.

Summarizing this ideal imaging picture one can say that the left-right on the CCD maps angle (in the horizontal plane) of the outgoing radiation while the up-down on the CCD convolves the wavelength with the angle in the vertical plane.

As usual with experimental work, life interferes with theoretical considerations. Alignment was performed for visible ($400nm$) light while detection was carried out for near UV ($300nm$). This difference in wavelength actually means a difference of $4.5mm$ in focal distance for the collimated lens. Thus light coming out of the lens was not strictly collimated. This means that the convolution of wavelength and the angle along the stripe (the up-down direction on the CCD) are extremely complicated. Furthermore, the diffraction grating was positioned at a slight angle with respect to ideal (groves are strictly horizontal). This resulted in a slight tilt of the stripe observed.

The focal distance of the lens was $10cm$ so 1cm left-right corresponds to .1rad. The CCD chip has 512 pixels for 1cm. Combining those facts we obtain a conversion of:

$$1PX = .195mrad \tag{4.1}$$

Figure 10 shows a typical experimental shot. The horizontal axis maps the angle (in the horizontal plane) of outgoing radiation. The vertical axis is a convolution of wavelength with the angle. The observed stripe is due to the interference of light from different loops of the radiating spiral. The stripe is tilted because the diffraction grating's groves are at an angle with the horizontal.

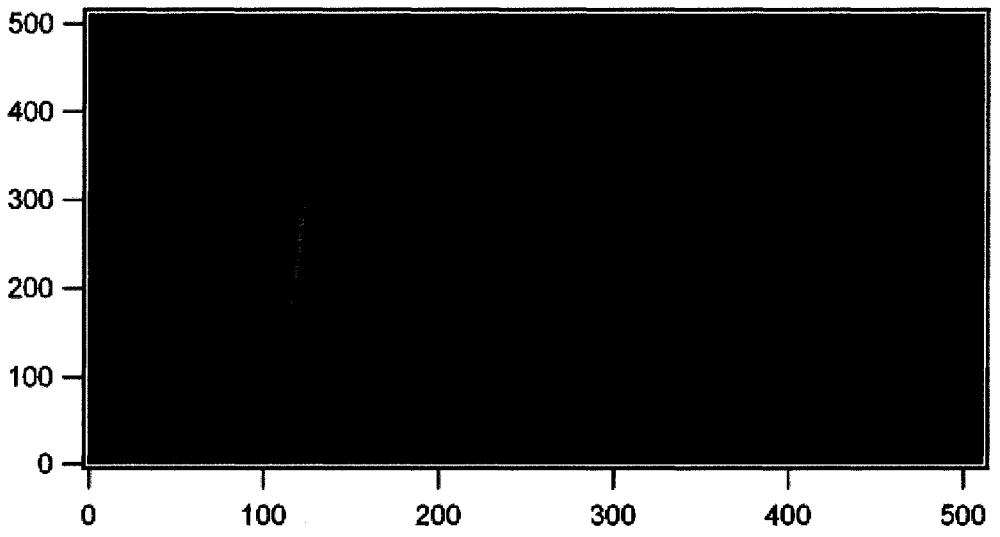

Figure 10. Experimental shot #3.

4.2. Data analysis method

An analysis method needed to be devised that would represent a single shot by an angle of synchrotron radiation. This angle, in turn, would help us judge the spatial coherence of the radiating electrons.

The data collected from the CCD presented a number of challenges. The shot-to-shot variance in CCD output was one of them. Finding the waist of the stripe (the up-down position on the CCD that corresponded to the narrowest point) was another one. Following is the procedure that was used to overcome those (and other) challenges.

First, data was binned vertically – instead of using 512 rows we used 51 each of which was the sum of ten original rows. This allowed us to overcome CCD shot-to-shot variance. The CCD output is an amplified result of the interaction between the photon and the silicon lattice. Those processes are stochastic, so binning reduces the role of chance in the further analysis, improving signal to noise ratio.

Along the horizontal axis data is expected to be Gaussian, because it is a result of N source constructive interference. Each of the 51 new "rows" was fitted a Gaussian. Figure 11 is the result of such fitting for shot #3 displayed above:

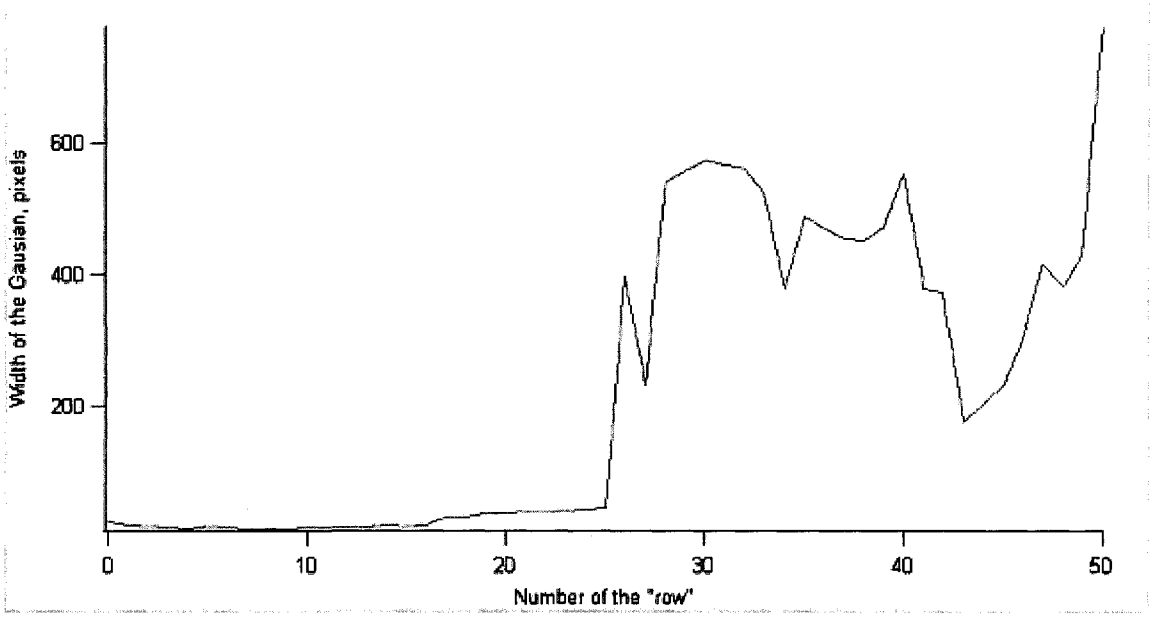

Figure 11. Fit results for shot #3.

The figure above consists of the plot of the width of the stripe (PX) vs. the number of the "row." Each "row" is a sum of ten lines of output of the CCD. In the right half of the plot, Gaussian fit produces absurd results because of very poor signal to noise ratios. In the left half there is a very well defined minimum ("row" number 10).

The minimum width of the plot corresponds to the vertical position where $300nm$ light produces the brightest, narrowest spot on the CCD. The next step is to attempt a special fit around the spot. This special fit is a sum of two Gaussians – one with a width of 50 pixels and the other with a width of 5 pixels We look for data rows with satisfactory fits. Figure 12 is an example of one such fit:

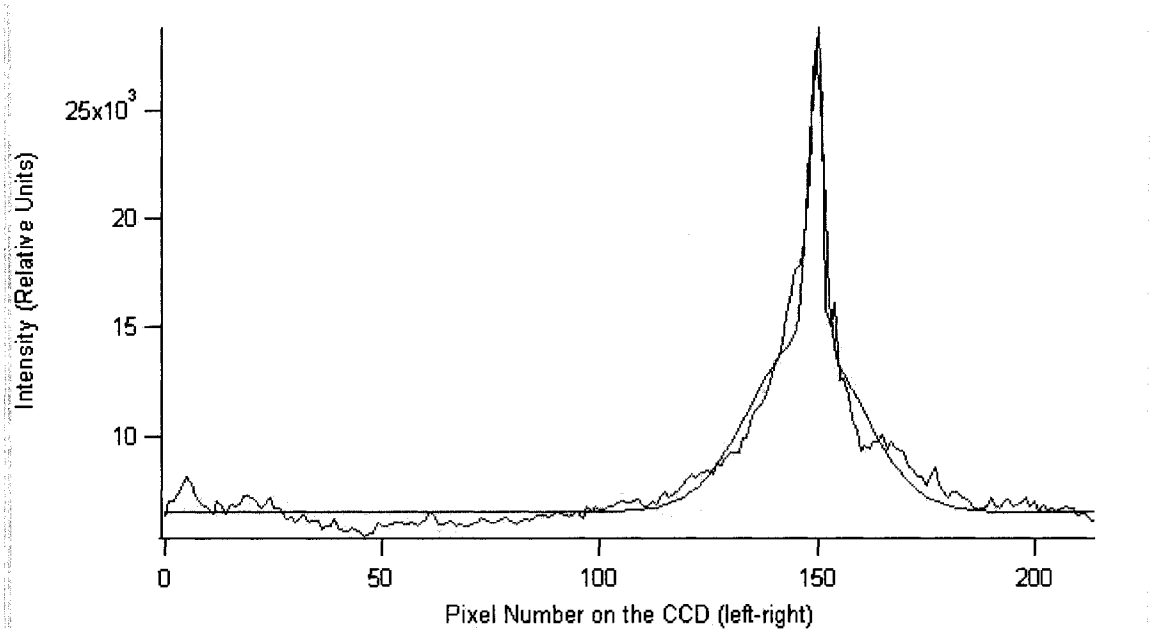

Figure 12. Secondary experimental fit for row #9 of shot #2.

The special experimental fit of the data gives us a Gaussian with a width of two pixels, translating into .7 *mrads*.

4.3. Results

Now it is time to present the experimental results. In the table below, five shots with circular polarization on the tungsten wire are presented. The energy of the shots is varied.

Table 3. Angular spread vs. Energy (the target is tungsten wire with circular polarization of the incident light)

SHOT #	1	2	3	4	5
Energy, mJ	602	839	780	849	245
Width (mrad)	1.43 ± 0.2	$.7 \pm 0.2$	$1.3 \pm .2$	1.9 ± 0.2	$1.7 \pm .2$

There were two sources of uncertainty in the values above. The first source stems from the Gaussian fits themselves – the Igor program gives out errors on the parameters of the fit (propagating those errors through the rest of analysis process is fairly straightforward). The second source of uncertainty is the fact that the CCD output is discrete. Our scaling is roughly 5PX per *mrad*, so uncertainty due to this factor is 1PX or $0.2 mrad$. Shots 1 and 2 had a Gaussian fit error significantly lower than that, so uncertainty due to the pixilation is prevalent. Figure 13 represents the angular spread for various shots.

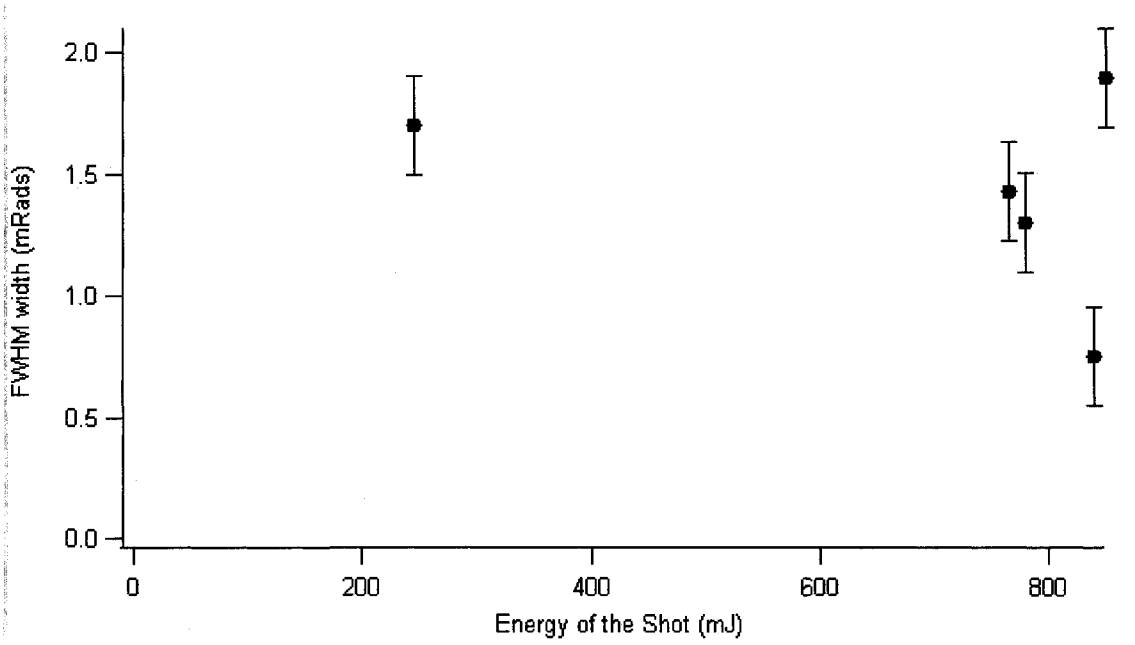

Figure 13. Angular spread vs. Energy of the shot

One additional shot added to the graph of the shots (shot #5 with energy $177mJ$) was done with linear polarization instead of circular. We still see a nice signal (as predicted in the end of 2.1 the Theory).

4.4. Discussion

The main result of the study presented here is that the synchrotron radiation was observed. This implies that a sufficient number of electrons is moving coherently.

Radiation detected by the CCD is a near-vertical, narrow band. This band is supposed to be vertical because our detection system maps wavelength and angle with respect to the horizontal onto the up-down direction on the chip. The angle between the band and the up-down direction is due to the fact that diffraction grating's grooves are

not perfectly horizontal as well as the fact that the CCD's chip is not perfectly aligned with the direction of the radiation. Finally, the narrowness of the band is determined by two effects. The first effect is interference – electrons radiating form a fairly long spiral, thus radiation emitted by electrons along the spiral interferes with itself. The second phenomenon affecting the width of the band is the fact that the collimating lens is slightly further than a focal distance away from the source, because of the $4.5mm$ focal length error. Thus, instead of being collimating after the lens, radiation is slightly converging, producing a narrow image on the CCD chip. Let's consider those geometrical features of the results in more detail.

One has to remember that the radiating spiral radiates light in all directions, perpendicular to the incoming laser beam (z-direction). This means that the whole length of the diffraction grating is lit by the narrow stripe of collimated light we are trying to detect. The CCD chip is situated so the first interference maximum hits it at a nearly normal incidence. The vertical stripe we see is the image (in the up-down direction) of the diffraction grating fully illuminated by the collimated radiation.

There is an extra stretching in the up-down direction. A slight deviation in wavelength would originally cause a slight angular deviation of the light after the diffraction grating. Our interference filter limits wavelength range accepted into the CCD down to $12nm$ (FWHM). This discrepancy in the wavelength ($12/300 = 0.004$) results in the appropriate discrepancy in the angle at which the radiation leaves the diffraction grating ($0.004 \cdot 30.5 = 0.122\,\text{deg} = 0.0021rad$). This, in turn, results in

displacement on the chip of $0.0021 \cdot 15.5cm = 0.03cm$. On the chip roughly 500 pixels constitute 1cm so this effect smears the result around 15 pixels in the vertical direction.

The stripe observed is at a slight (.15rad) angle with the up-down direction. This is due to the misalignment of the grating and the CCD. The design called for those elements to be aligned along the focal spot – lens – mirror direction, with grating's grooves to be horizontal and perpendicular to that direction. Unfortunately, additional demands (primarily on how rigid the whole construction must be) precluded the setup from having the perfect alignment. The grating and the CCD were not rigidly connected, thus slight misalignments of the setup accumulated to produce the relative tilt observed.

Perhaps the most striking feature of the results is how narrow the radiating band is. In Chapter 2, we derived the theoretical value of $3mrad$. Experimental results range between $2mrad$ and $4mrad$. This is fairly good agreement. However, some of the experimental results are actually better than theory would predict. This difficulty is explained by the difference between the theoretical assumptions and the experimental setup.

The theoretical value of $3mrad$ is computed assuming that the interfering light is collimated by the lens. This is not exactly true. The lens was positioned to perfectly collimate visible light ($\lambda = 450nm$). During the experiment we detect light of a different wavelength ($\lambda = 300nm$). Glass from which the lens is made (BK7 grade) has different refraction indices for those two wavelengths:

$\lambda_{300} = 1.5253$
$\lambda_{450} = 1.5527$

This difference results in the difference in focal distances, namely for $300nm$ the focal distance of our lens is longer. Elementary optics states that the focal distance of the lens is inversely proportional to the index of refraction. The difference in the refraction indices for different wavelengths means that our lens has a focal length which is 1.8 percent shorter for the light detected compared with the light aligned. This results in the light converging (instead of being perfectly collimated). Figure 14 gives the geometrical picture.

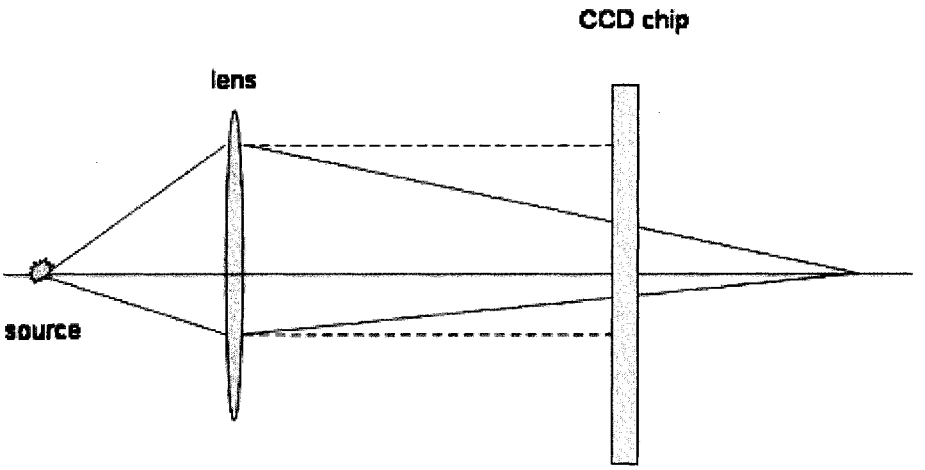

Figure 14. Difference between theoretical (dashed lines) and experimental (solid lines) paths of light.

It is clear to see that during the experiment, the source is slightly behind the focal point of the lens.

Elementary optics calculations put the point where the source is really imaged at $565cm$ after the lens. The geometrical setup of the experiment gives a lens-CCD distance of $100cm$. Thus the theoretical value needs to be corrected correspondingly:

$$Size = Size(theory) \cdot \frac{565 - 100}{565} = 2.47mrad$$

The value above is considerably more in the agreement with the experimental results. In conclusion, the fact we see anything on the CCD output proves the main point of the thesis: intense laser light drives electrons, thus making them radiate coherently. The area of the space where this occurs is fairly large (up to a fifty wavelengths of incoming laser light). Furthermore all the peculiarities of the picture on the CCD are explainable through geometric and other phenomena discussed here.

5.0. CONCLUSION

Plasma-light interactions for high energy ultra-short pulses produce detectable broadband radiation. This radiation has been successfully detected at a wavelength of $300nm$. Careful studies allow us to discard all other explanations for the radiation detected.

The broadband radiation is emitted by laser-driven electrons in the plasma. Depending on the polarization of the light, electrons exhibit either circular (circular polarization) or figure 8 (linear polarization) orbits. The linear dimensions of the orbits are on the order of $1\mu m$. Those orbits require electrons to accelerate and accelerating charges always radiate. The driving laser pulse is Gaussian in time so the electrons' movement is not purely harmonic. This is why radiation is emitted as broadband.

The radiation detected is directional. This radiation is mostly at a right angle with the direction of laser propagation (called the z axis in the geometry of this work). To be specific, the radiation diverges slightly (up to $2.2mrad$) from the z axis. In the case of circular polarization the whole problem is cylindrically symmetrical, so the broadband radiation emitted is viewed as a slightly diverging disc perpendicular to the z axis.

The low angular divergence of the radiation is due to the constructive interference. This means that the sources of the radiation are coherent. Electrons driven by laser light have similar orbits over sufficient length of space ($40\mu m$ along the z axis) for interference to narrow down the outgoing radiation.

Both circular and linear polarizations are observed to emit this broadband radiation. The different polarizations of the driving light result in the different orbits of the radiating electrons. This is the main reason the radiation is much easier to detect when the electrons are driven by the circularly polarized light.

There are several important measurements still to be done on the laser-plasma interaction. Radiation detected apparently is emitted in a thin disc perpendicular to the propagation of the laser pulse. The narrowness of this disc is attributed to the interference of the radiation emitted by electrons. What we are measuring is width of the zeroth order maximum. Extremely interesting would be observation of higher order maxima. Existence of such maxima would solidify the claim that we have interference off the emitted radiation. Directions towards those maxima, as well as the maxima's widths, would supply us with additional data on the geometry and dynamics of the radiating electrons.

Additional insights into intricacies of the laser-plasma interaction could be provided by measuring the polarization of the radiation emitted. Let us assume the radiation emitted is polarized along a certain direction. That would limit the types of motion that electrons could possible be undergoing. For a moving charge, the polarization is determined by direction of velocity and acceleration. Thus, knowing the polarization of the radiation emitted would provide us with significant additional clues to the electrons' movement.

Other highly desirable quantities to measure are plasma temperature and density at the point of laser-plasma interaction. Those parameters are indispensable in obtaining a clearer picture.

There are several interesting features that make the experiment an intriguing UV light source. The duration of the radiation, its directionality and the fact that this radiation is broadband are among those features. The electrons radiate only when they are driven by the laser light. The laser pulse in our experiment is around $140\,fs$. Thus we conceivable emit out a broadband pulse of the same duration. Furthermore, there are laser systems in the world with pulse durations as short as $50\,fs$. Any imaging device based on the phenomenon discussed in this work would allow for time resolution of the processes imaged on the same timescales. Strobe imaging of chemical reactions is one of the obvious candidates. Time-resolving biochemistry of living cells is another.

The fact that the radiation is broadband means that one has considerable freedom to chose which wavelength of the radiation to utilize when using laser driven electrons as the source. This freedom should greatly facilitate the imaging discussed above – freedom to choose wavelength to backlight certain chemical compounds means great certainty that one is observing the molecules one needs to observe.

One of the more surprising features of the radiation detected is its high directionality (a spread of around $2mrad$ around the direction perpendicular to laser

pulse propagation). This high directionality, coupled with a fairly small size (around 40*microns*) contributes towards making sources like that ideal candidates for microscopy. Lastly, the broadband radiation emitted falls into a convenient part of the electromagnetic spectrum – mirrors reflect it well, there are materials from which efficient lenses could be made, etc.

Finally, the process under consideration produces photons in sufficient numbers for detection. After all, what use would the source be if, despite all its good qualities, it were still too dim to make an image? The study presented here proves that laser driven electrons radiate enough photons for successful detection.

On a less utilitarian note, it is important to continue experiments studying plasmas created by ultra-short laser pulses. Plasmas are notoriously hard to model due to the number of interacting particles and multitudes of effects taking place. However, the advancement of knowledge about plasmas seems important for several reasons. First, the addition to humankind's knowledge base is always an admirable goal in itself. Second, there are several areas of physics where plasmas play an important role. One example is astrophysics – plasmas are found everywhere from the cold interstellar regions to the burning cores of the stars. Lastly, knowledge about extreme states of matter is relevant in nuclear engineering.

REFERENCES

Esarey, E. Ride, S.K. and Sprangle, P. (1993). Nonlinear Thomson scattering of intense laser pulses from beams and plasmas, *Physical Review Letters E*, 48, 3003-3021.

Garrett, W.R. (2002). Comment on Lasetron: a proposed source of powerful nuclear-time-scale electromagnetic bursts, *Physical Review Letters*, 89, 279501-1.

Jackson, J.D. (1998). *Classical electrodynamics* , Hoboken, New Jersey: John Wiley and Sons, Inc.

Kaplan, A.and Shkolnikov, P. (2002). Lasetron: a proposed source of powerful nuclear-time-scale electromagnetic bursts. *Physical Review Letters*, 88, 074801-1 – 074801-4.

Kaplan, A. and Shkolnikov, P. (2002). A Reply to the comment by G. Stupakov and M. Zolotorev. *Physical Review Letters*, 88, 199502-1.

Kaplan, A. and Shkolnikov, P. (2002). A Reply to the comment by W.R.Garret. *Physical Review Letters*, 88, 279502-1.

Landau, L. and Lifshiz, E. (1975). *Classical field theory*, New York, New York: Pergamon.

Lee, K. et al., (2003). Relativistic nonlinear Thomson scattering as attosecond x-ray source, *Physical Review Letters E*, 67, 026502-1 – 026502-7.

Lee, K. Kim, B.H. and Kim, D. (2005). Coherent radiation of relativistic nonlinear Thomson scattering, *Physics of Plasmas*, 12, 043107-1 – 043107-8.

Sarachik, E.S. and Shappert, G.T. (1970). Classical theory of the scattering of intense laser radiation by free electrons, *Physical Review Letters D* 1, 2738-2753.

Stupakov, G. and Zolotarev, M. (2002). Comment on Lasetron: a proposed source of

powerful nuclear-time-scale electromagnetic bursts, *Physical Review Letters*, 89, 199501-1.

Wharton, K.B. and MacKinnon, A. (2002). Synchrotron radiation from intense circulary-polarized light, ILSA grant proposal.